NAVAL POSTGRADUATE SCHOOL

MONTEREY, CALIFORNIA

THESIS

CORRECTING SURFACE FIGURE ERROR IN IMAGING SATELLITES USING A DEFORMABLE MIRROR

by

James J. Watson

December 2013

Thesis Co-Advisors: Brij Agrawal
Jae Jun Kim

THIS PAGE INTENTIONALLY LEFT BLANK

REPORT DOCUMENTATION PAGE			*Form Approved OMB No. 0704-0188*
Public reporting burden for this collection of information is estimated to average 1 hour per response, including the time for reviewing instruction, searching existing data sources, gathering and maintaining the data needed, and completing and reviewing the collection of information. Send comments regarding this burden estimate or any other aspect of this collection of information, including suggestions for reducing this burden, to Washington headquarters Services, Directorate for Information Operations and Reports, 1215 Jefferson Davis Highway, Suite 1204, Arlington, VA 22202-4302, and to the Office of Management and Budget, Paperwork Reduction Project (0704-0188) Washington DC 20503.			
1. AGENCY USE ONLY ***(Leave blank)***	**2. REPORT DATE** December 2013	**3. REPORT TYPE AND DATES COVERED** Master's Thesis	
4. TITLE AND SUBTITLE CORRECTING SURFACE FIGURE ERROR IN IMAGING SATELLITES USING A DEFORMABLE MIRROR			**5. FUNDING NUMBERS**
6. AUTHOR(S) James J. Watson			
7. PERFORMING ORGANIZATION NAME(S) AND ADDRESS(ES) Naval Postgraduate School Monterey, CA 93943-5000			**8. PERFORMING ORGANIZATION REPORT NUMBER**
9. SPONSORING /MONITORING AGENCY NAME(S) AND ADDRESS(ES) N/A			**10. SPONSORING/MONITORING AGENCY REPORT NUMBER**
11. SUPPLEMENTARY NOTES The views expressed in this thesis are those of the author and do not reflect the official policy or position of the Department of Defense or the U.S. Government. IRB protocol number ____N/A____.			
12a. DISTRIBUTION / AVAILABILITY STATEMENT Approved for public release; distribution is unlimited			**12b. DISTRIBUTION CODE** A
13. ABSTRACT (maximum 200 words) A deformable mirror is proposed as a solution to correct aberrations on a satellite primary mirror surface. The deformable mirror is used in a double-pass configuration with an interferometer and a mirror segment on the Naval Postgraduate School Segmented Mirror Telescope to test the ability of a deformable mirror to correct inherent surface figure aberrations of an imaging satellite mirror surface. Manual, iterative feedback, and constrained optimization control methods are used to control the deformable mirror to correct surface figure error on the Segmented Mirror Telescope mirror segments to achieve 55% root mean square improvement for the primary mirror segment surface.			
14. SUBJECT TERMS Segmented mirror telescope, adaptive optics, deformable mirror, surface figure error			**15. NUMBER OF PAGES** 75
			16. PRICE CODE
17. SECURITY CLASSIFICATION OF REPORT Unclassified	**18. SECURITY CLASSIFICATION OF THIS PAGE** Unclassified	**19. SECURITY CLASSIFICATION OF ABSTRACT** Unclassified	**20. LIMITATION OF ABSTRACT** UU

NSN 7540-01-280-5500

Standard Form 298 (Rev. 2-89)
Prescribed by ANSI Std. 239-18

THIS PAGE INTENTIONALLY LEFT BLANK

Approved for public release; distribution is unlimited

CORRECTING SURFACE FIGURE ERROR IN IMAGING SATELLITES USING A DEFORMABLE MIRROR

James J. Watson
Commander, United States Navy
B.S., United States Naval Academy, 1997
M.A., Naval War College, 2007

Submitted in partial fulfillment of the
requirements for the degree of

MASTER OF SCIENCE IN ASTRONAUTICAL ENGINEERING

from the

NAVAL POSTGRADUATE SCHOOL
December 2013

Author: James J. Watson

Approved by: Brij Agrawal
Thesis Co-Advisor

Jae Jun Kim
Thesis Co-Advisor

Knox Millsaps
Chair, Department of Mechanical and Aerospace Engineering

THIS PAGE INTENTIONALLY LEFT BLANK

ABSTRACT

A deformable mirror is proposed as a solution to correct aberrations on a satellite primary mirror surface. The deformable mirror is used in a double-pass configuration with an interferometer and a mirror segment on the Naval Postgraduate School Segmented Mirror Telescope to test the ability of a deformable mirror to correct inherent surface figure aberrations of an imaging satellite mirror surface. Manual, iterative feedback, and constrained optimization control methods are used to control the deformable mirror to correct surface figure error on the Segmented Mirror Telescope mirror segments to achieve 55% root mean square improvement for the primary mirror segment surface.

THIS PAGE INTENTIONALLY LEFT BLANK

TABLE OF CONTENTS

LIST OF FIGURES

THIS PAGE INTENTIONALLY LEFT BLANK

LIST OF TABLES

THIS PAGE INTENTIONALLY LEFT BLANK

LIST OF ACRONYMS AND ABBREVIATIONS

BMC	Boston Micromachines Corporation
CFRP	carbon fiber reinforced polymer
CGH	computer-generated hologram
CP	circularly polarized
DM	deformable mirror
IC	intelligence community
IFCO	iterative feedback constrained optimization
ISR	intelligence surveillance reconnaissance
JWST	James Webb space telescope
MEMS	micro-electro-mechanical systems
NASA	national air and space administration
NRO	national reconnaissance office
OPD P-V	optical path difference peak to valley
PBS	polarized beam splitter
RMS	root mean square
SMT	segmented mirror telescope

THIS PAGE INTENTIONALLY LEFT BLANK

ACKNOWLEDGMENTS

I am very grateful for the guidance and mentorship of Distinguished Professor Brij Agrawal, and the opportunity he gave me to join his top-notch team in the Adaptive Optics Center of Excellence. My colleagues in AOCoE were inspiring, and taught me the discipline and joy of research.

I am thankful for Dr. John Bagnasco's countless hours of optics mentorship and his drive for excellence. Dr. Jae Jun Kim's engineering knowledge and untiring work ethic kept me moving forward. Dr. Ty Martinez constantly turned optical ideas into physical reality. Dr. Bautista Fernandez and Travis Axtell gave me invaluable assistance with optical alignment and MATLAB. CAPT Al Scott, Dr. Edwin Ahn, MAJ Matt Allen, Mike Krol, Albert Jordan, Dr. Lew Desandre, LT Lee Johnson, and Ms. Eva Carrillo kept me grounded while somehow managing to motivate me every day.

I am especially thankful for my family's encouragement, understanding, and patience with the constant phrase, "Going to the lab—be back in a while."

THIS PAGE INTENTIONALLY LEFT BLANK

I. INTRODUCTION

The Intelligence Community (IC) desires greater resolution and more persistence in national space-based Intelligence Surveillance Reconnaissance (ISR) systems. Greater resolution and persistence require imaging satellites with larger primary optics and higher orbits than are currently available. Segmented mirror concepts, as seen in Figure 1, move beyond the size and weight limits of current optical systems and divide over-sized optics into smaller lightweight mirrors that can work in tandem as a single large optic. Light segmented mirror segments could be unfolded and precisely controlled on orbit to provide a leap forward in ISR capability.

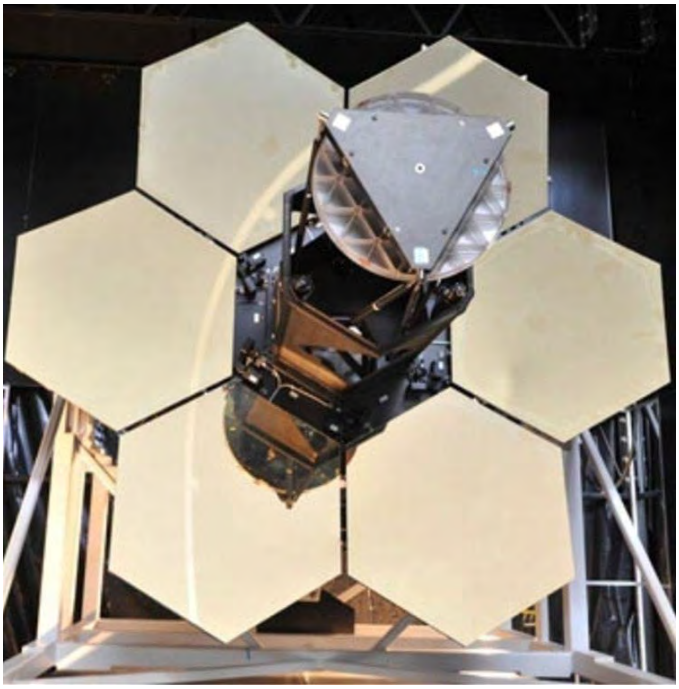

Figure 1. NPS segmented mirror telescope (from [1]).

A. PURPOSE

Segmented mirror systems introduce new complexities and technological issues that require novel approaches and solutions. The issue of potential mirror surface figure aberrations induced by control system interaction or structural components must be

addressed in order to confidently launch a segmented mirror system into orbit. The goal of this thesis is to provide a proof-of-concept for an integral component that would serve as a mirror surface figure corrector to enable the ultimate goal of confidently launching a segmented mirror imaging satellite.

1. Experiment

The study will be a center of curvature experiment in which a deformable mirror is placed in a double pass configuration with an interferometer to correct for the wave front error on a segmented mirror. The study will focus on the feasibility of using a deformable mirror to correct wave front aberrations caused by imperfections on the segmented mirror surface.

2. Approach

This experiment will utilize the Segmented Mirror Telescope (SMT) control actuators in a static mode. Alternatively stated, the control configuration of the SMT segment will be fixed for a given surface figure, and all corrections to the surface figure will be made using the deformable mirror. This approach will isolate the performance of the deformable mirror in its ability to correct surface figure aberrations for segmented mirrors. The best surface figure that can be achieved by a mirror segment with its 156 face sheet actuators will be taken as the baseline, and then that baseline will be used with a deformable mirror in the loop to attempt to improve the mirror surface figure.

B. OVERVIEW

Chapter II provides background understanding about the Naval Postgraduate School's SMT test-bed and the required performance for mirror surface figures. The experimental set-up, including the optical path, interferometer, deformable mirror, and mirror segment, are explained in Chapter III. Chapter IV covers the deformable mirror in greater detail, describing its configuration and operation. Control methods, including influence matrix development and control laws used for the experiment, are provided in Chapter V. Experimental results, data, and analysis are given in Chapter VI. Chapter VII concludes with recommendations for further work.

II. BACKGROUND

Segmented mirror technology will open the door to a new era of space-based imagery. In addition to ISR, the astronomy community will soon use segmented technology in advanced projects such as National Aeronautical Space Administration's (NASA) follow-on for the Hubble Space Telescope, the James Webb Space Telescope (JWST) [2]. In addition to higher performance, segmented mirror satellites will be more economical and more operationally responsive than current imaging satellites. The decreased manufacture time and decreased weight of smaller mirror segments that replace the primary optic will dramatically reduce production timelines and material expense, thus providing increased ISR capability at lower overall cost.

The National Reconnaissance Office (NRO) developed an experimental segmented mirror telescope as a proof-of-concept for segmented mirror technology [3]. The technology demonstrator, now known as the Segmented Mirror Telescope, is hosted at the Naval Postgraduate School. Larger than the Hubble Space Telescope, but smaller than the JWST (see Figure 2), the SMT is an advanced test-bed to research the diverse technology areas that comprise a segmented telescope system [1].

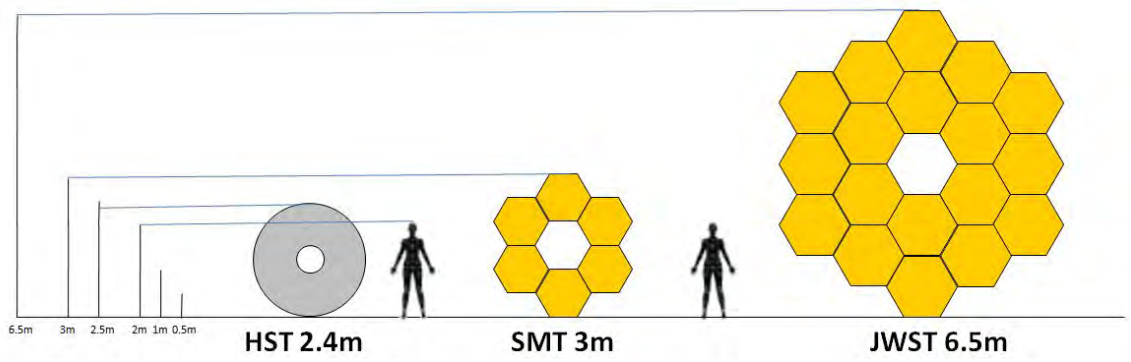

Figure 2. Comparison of SMT to Hubble and James Webb space telescope (from [1]).

A. SEGMENTED MIRROR CONFIGURATION

Six equally-sized hexagons on the SMT form a primary mirror surface. In their un-stowed, operational position, the mirrors are arranged to fit together in an orientation that looks similar to a traditional primary mirror (see Figure 3). The segmented mirror can be folded for launch and mechanically unfolded by means of hinges connected to paired segments [3].

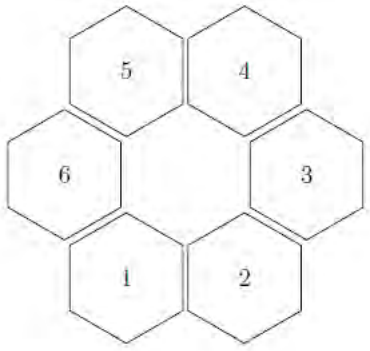

Figure 3. NPS SMT segmented mirror orientation (from [3]).

The six segments of the primary mirror have a lightweight, deformable, nano-laminate face with actuators across the rear surface for controlling the surface shape of the mirror segments as seen in Figure 4.

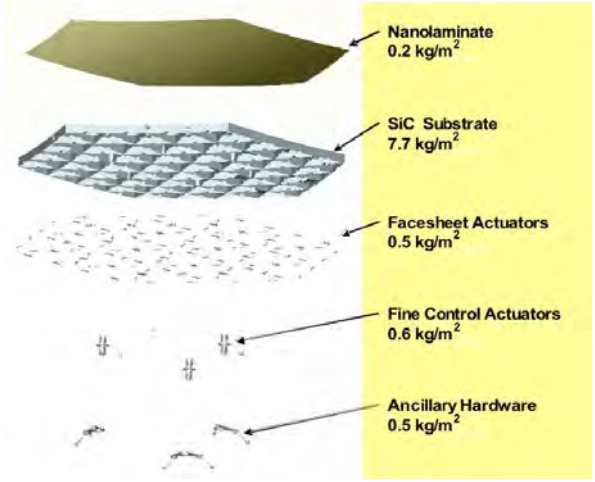

Figure 4. Segment composition (from [1]).

Three types of actuators perform functions from major to minor movement. From low order to high order, these three actuators are the coarse actuators (lowest order or "coarse" corrections), fine actuators, and face sheet (highest order) actuators. The coarse and fine actuators provide rigid body motion to the segments. The face sheet actuators are used to correct the segment surface. The system could be considered an "active" optics system since it is correctable, but it is not a true "adaptive" optics system because the system does not correct the wave-front in high temporal frequency [3].

B. SEGMENT SURFACE FIGURE

A single segment requires a very high quality surface figure in order to be of optical quality at geostationary orbital range. For a diffraction-limited optic, performance is maintained for up to a quarter-wave of optical path difference peak to valley (OPD P-V) which corresponds to a root mean square (RMS) wave-front error of $\lambda/14$ [4]. The current SMT surface figure has aberrations, diminishing the surface figure to 0.46 waves RMS, as seen in figures 5 and 6. The goal of this experiment will be to reduce the aberrations on the mirror segment as much as possible to decrease the current value of 0.46 waves RMS.

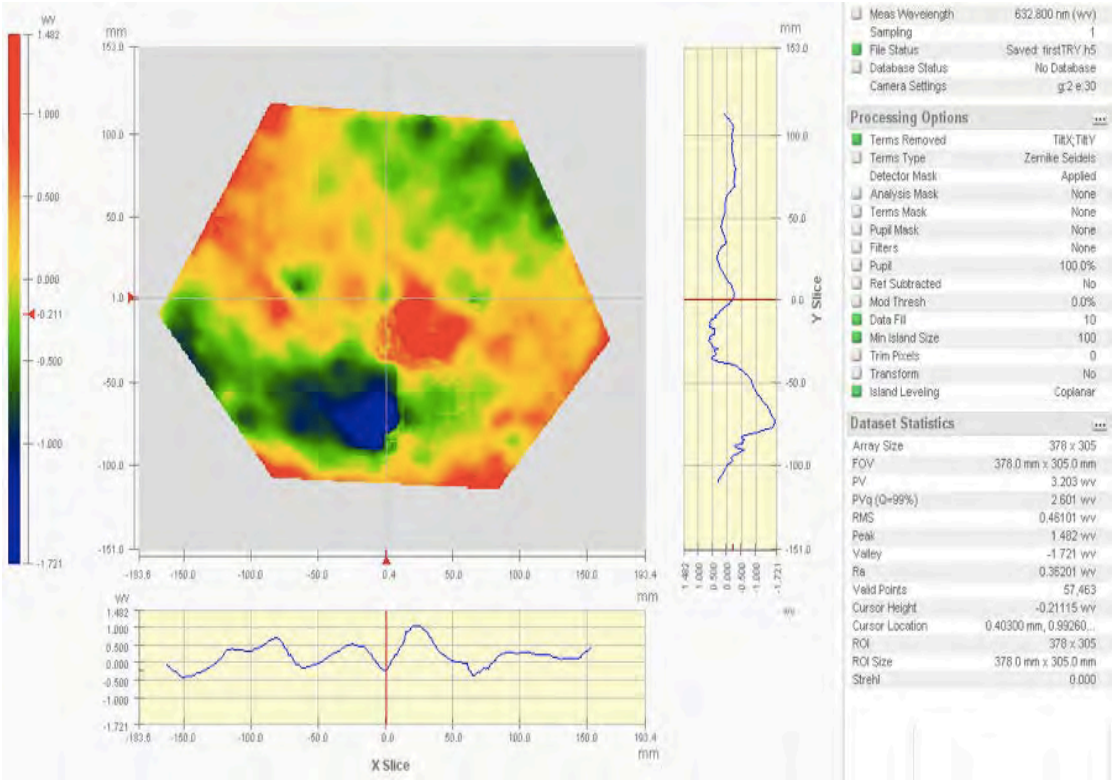

Figure 5. Mirror segment surface figure aberrations as viewed by interferometer.

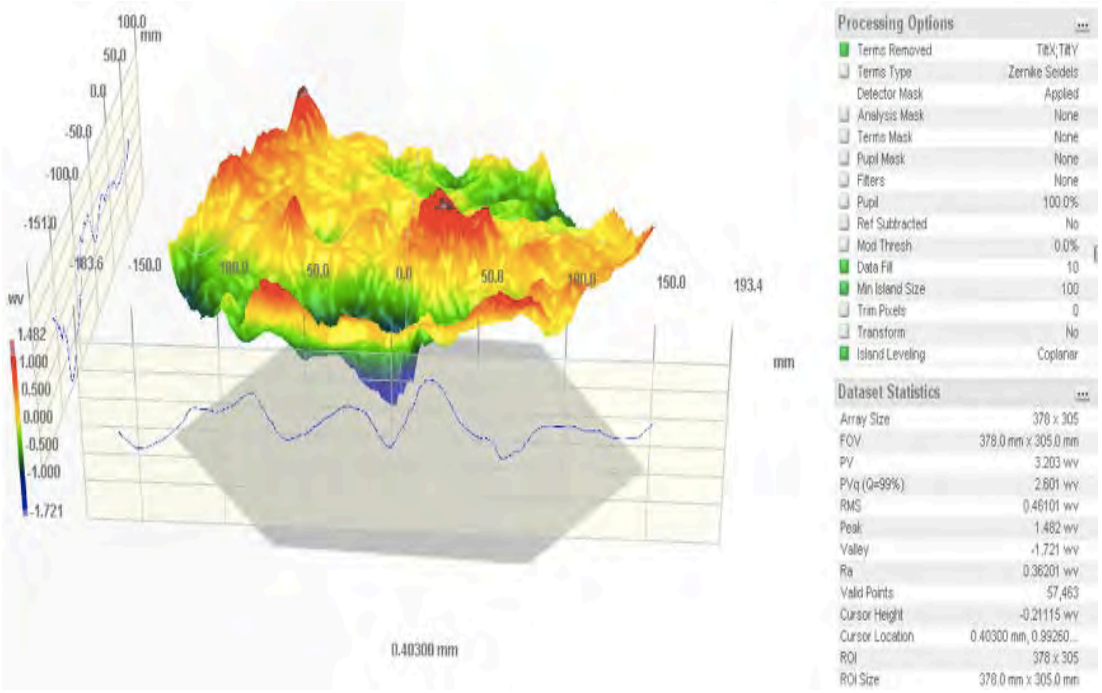

Figure 6. Three-dimensional rendering of surface figure aberrations in waves.

III. EXPERIMENTAL SET-UP

A. EXPERIMENTAL CONCEPT OVERVIEW

The configuration utilized for this deformable mirror experiment is a modification of a previous center of curvature experiment on the SMT test-bed, as seen in Figure 7. Research scientists used an interferometer and computer generated hologram (CGH) to assess and attempt to improve the quality of the SMT mirror segments. An additional optical path was added to the original experiment to place the deformable mirror in the optical configuration to affect the segment's surface figure quality [5].

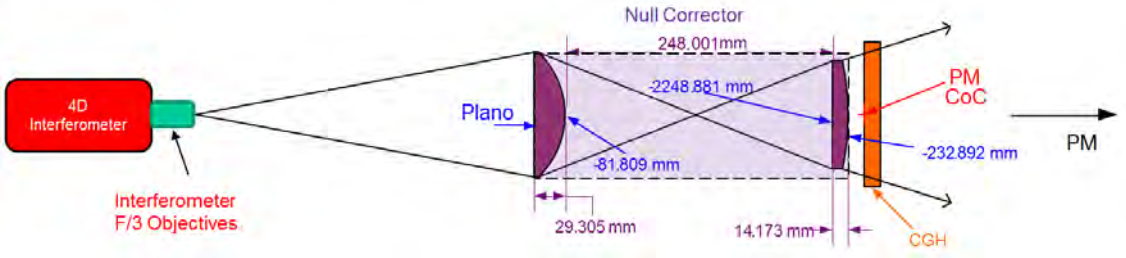

Figure 7. Original SMT center of curvature experiment (after [5]).

The high-level concept of adding the deformable mirror in Figure 8 is represented as an adaptation of Figure 7. In practice, the configuration including a deformable mirror is more complex to implement than the basic schematic shows, and the details of the optical path warrant further explanation in the following chapter.

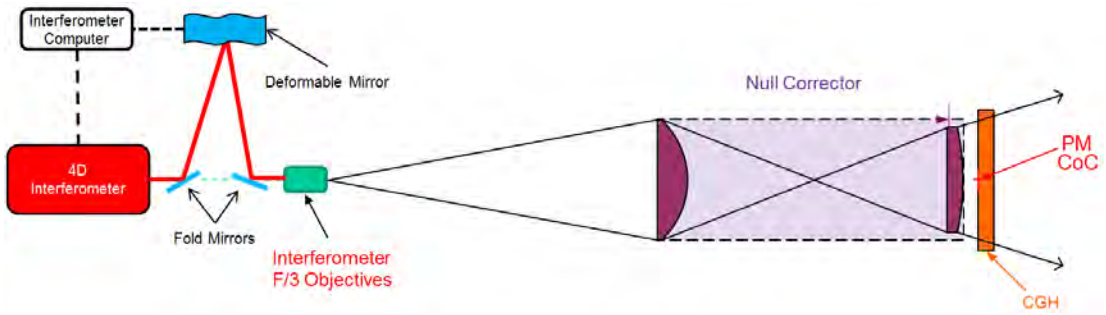

Figure 8. Modified center of curvature experiment with deformable mirror (from [5]).

B. OPTICS PATH

1. Configuration for Viewing Mirror Segment with DM in Path

The additional optics path that was added to accommodate the addition of a deformable mirror is comprised of an optical relay, a polarized beam splitter (PBS) and three ¼ wave plates. The additional relay moves the pupil plane from the f/3 objective to the deformable mirror, and then to the interferometer. In order to provide a CGH/SMT segment higher contrast return signal, the wave-plates and polarizers are used to reduce reflections from the relay optics, as seen in Figure 9.

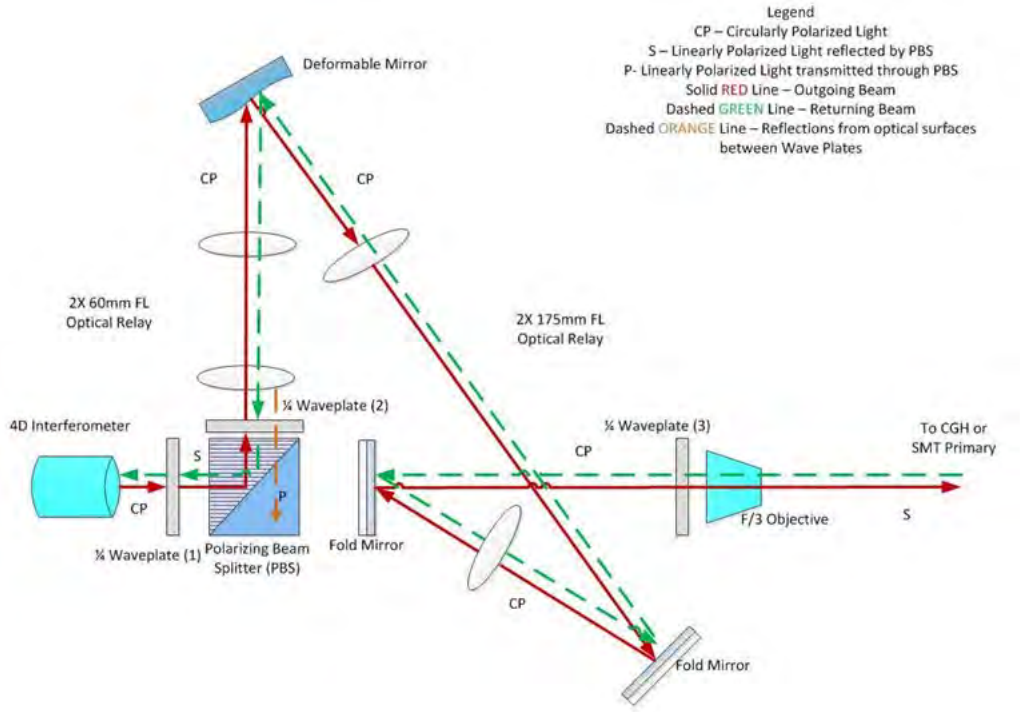

Figure 9. Deformable mirror sub-assembly schematic (from [6]).

The pupil plane of the interferometer is relayed to the deformable mirror by two 60 mm focal length achromatic doublet relays. From the DM, two 175 mm focal length achromatic doublets are used to relay the path to the f/3 objective, with two fold mirrors being added to obtain proper path length.

Anti-reflection components are included in the DM sub-assembly to eliminate unwanted back reflections. A ¼ wave-plate is used after the interferometer to convert circularly polarized (CP) light to linearly polarized light, with a rotated alignment for S polarization. The S-polarized light leaving the ¼ wave-plate is then reflected with a polarized beam splitter (PBS) to relay only S-type light to the next ¼ wave-plate, as seen in Figure 10.

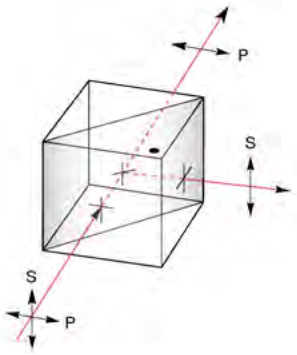

Figure 10. Polarized beam splitter reflects the linearly polarized beam into separate S and P polarization components (from [6]).

The S polarized light is converted back to circularly polarized light after passing through the second ¼ wave-plate. The light is again converted to S polarization after passing two optical relays and two fold mirrors and a third ¼ wave-plate. After the final ¼ wave-plate, the light reaches the f/3 objective lens where it is expanded. The expanded light leaving the f/3 objective travels to the SMT mirror segment and is reflected back to sub-assembly following the same path which it previously traversed, as seen in Figure 11. The final destination of the optical path is also the origination point, the 4D interferometer. On the return path, back-reflections are avoided by the polarization of the light. The back-reflected light that passes through the second wave-plate is converted to P polarization light, and therefore is not reflected through the PBS to the interferometer [6].

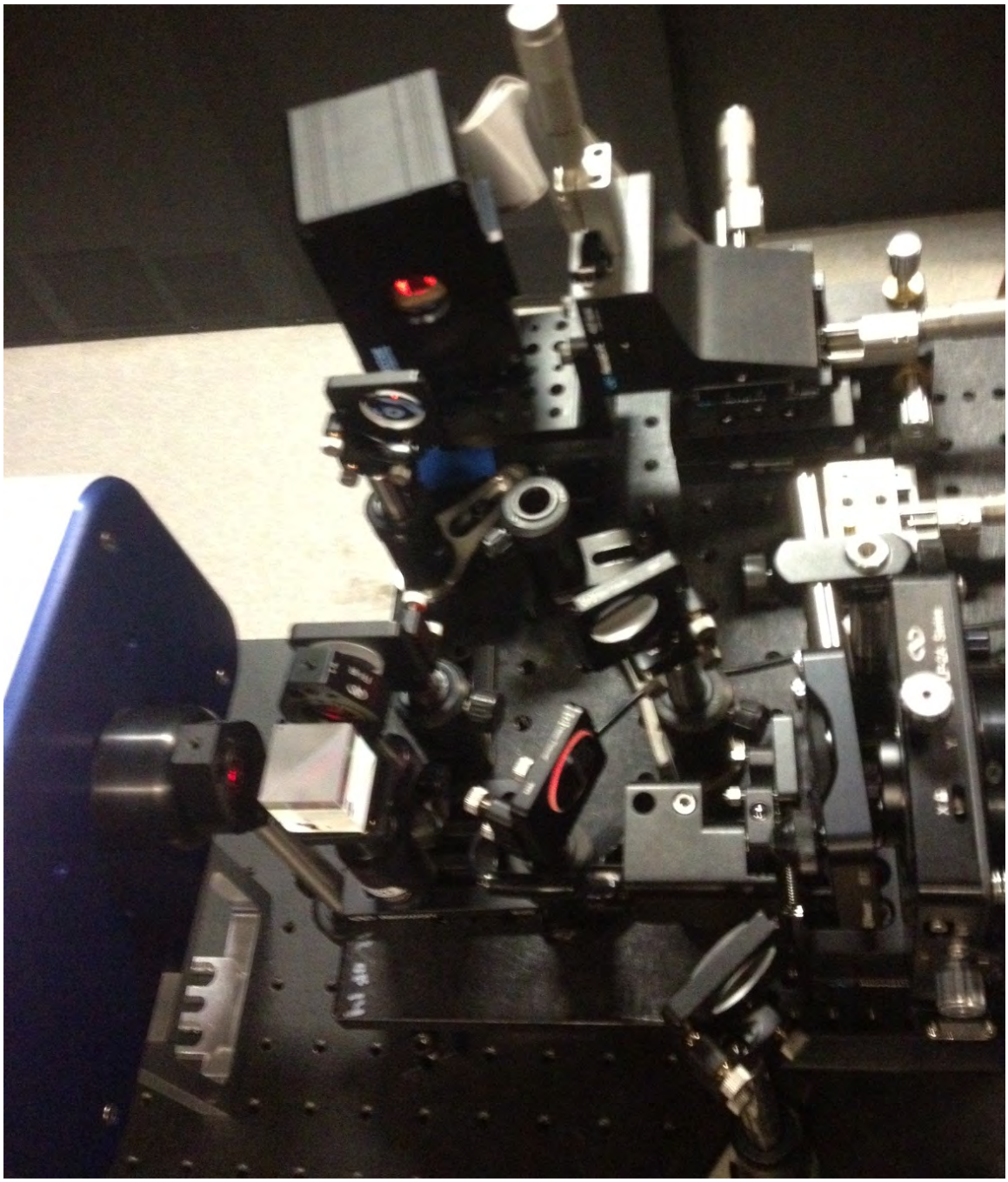

Figure 11. Top view of DM sub-assembly in optical path.

2. Configuration for Collecting Influence Function Data

An additional modification to the DM subassembly, as seen in Figure 12, was required in order to accommodate the collection of influence function data. For influence function data collection, the interferometer needs to be in view of the deformable mirror without the mirror segment being in the optical path. To collect accurate influence functions, it is imperative to only have the deformable mirror create the interferometer sensor output, without the mirror segment image being overlaid. To do this, a flip mirror would need to be installed which gives the option to switch the mirror segment out of the path when collecting influence function data.

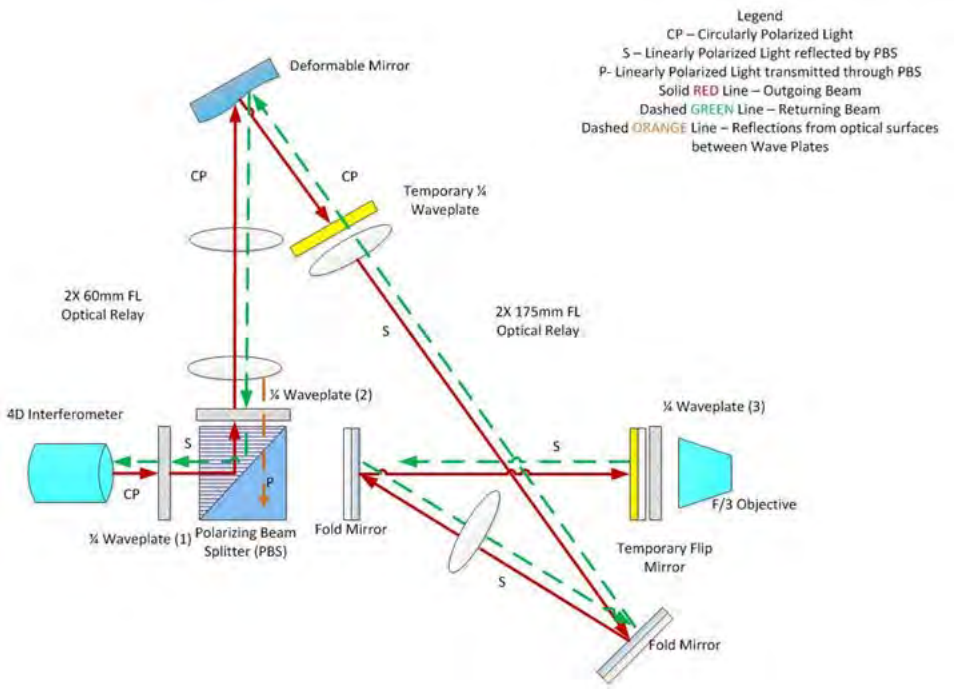

Figure 12. Influence function configuration with flip mirror (from [6]).

With the flip mirror installed, the f/3 pupil plane is relayed back to the deformable mirror and interferometer. In order to transmit through the 175 mm relay, but eliminate reflections from the 60 mm relay, a temporary wave-plate is also installed when influence functions are being collected [6].

3. 4D Interferometer

The 4D Interferometer, as seen in Figure 13, measures the shape of optical surfaces with extreme accuracy. Unlike a conventional interferometer that uses phase-shifting interferometry for measurement, the 4D interferometer uses proprietary, high resolution, high speed wave-front sensors to perform "dynamic" interferometry. The technology for the 4D interferometer was developed in cooperation with NASA for use with testing the James Webb Space Telescope. In phase-shifting interferometers, vibration and turbulence can degrade measurements as frames of data are acquired over many milliseconds. However, in a dynamic interferometer, all phase data are acquired simultaneously. The ability to collect data in extremely short intervals, as fast as 30 microseconds, allows the 4D dynamic interferometer in the experiment optical path to make extremely accurate measurements in the presence of potential vibration or slight air turbulence [7]. The interferometer was mounted on an experiment table above a hexapod, as seen in Figure 14.

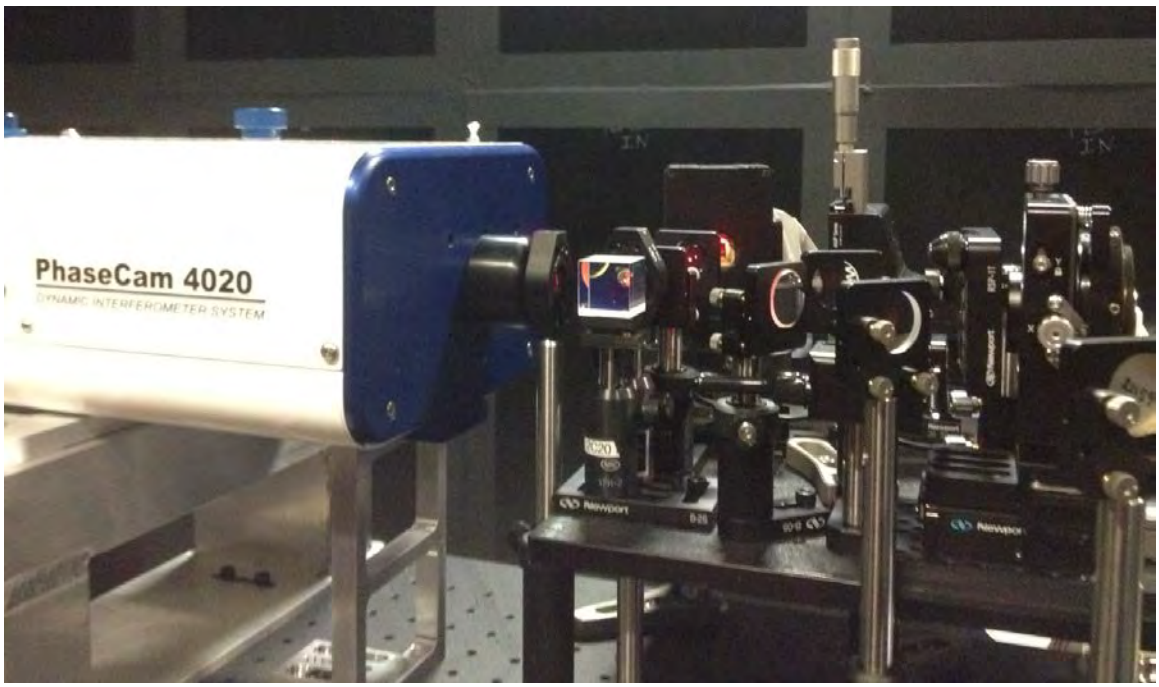

Figure 13. Interferometer and optical path side view.

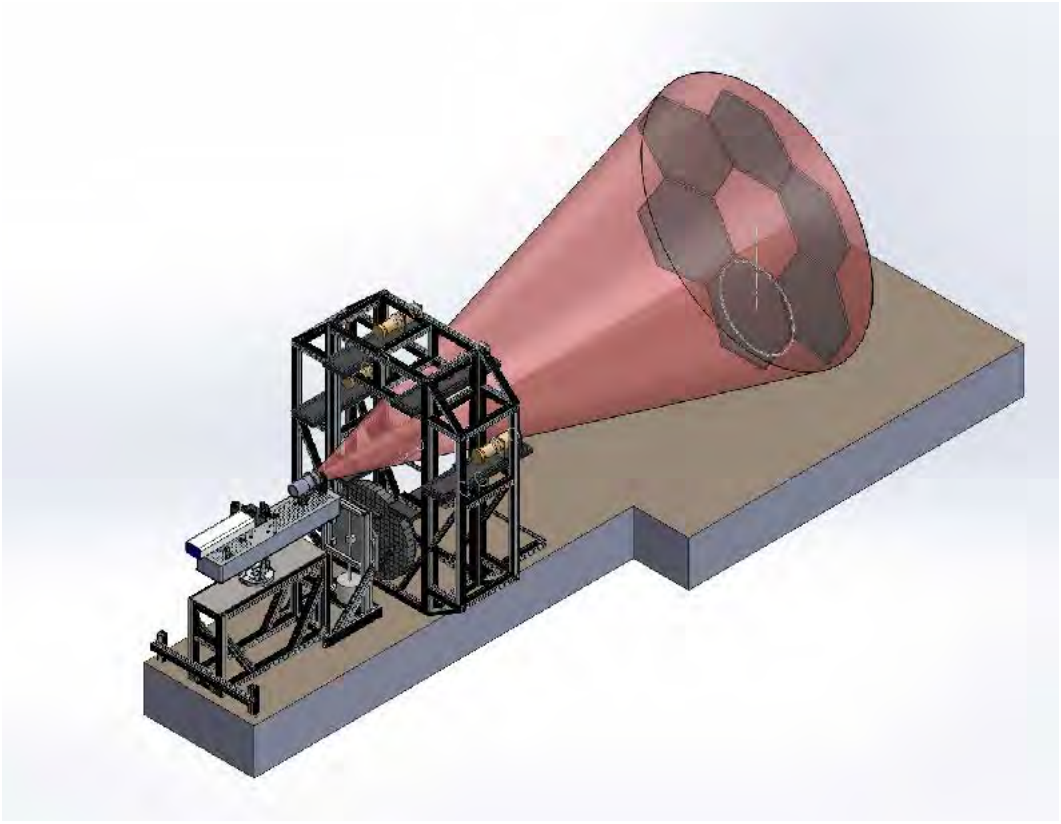

Figure 14. Experimental set-up including light path to mirror segment (from [8]).

THIS PAGE INTENTIONALLY LEFT BLANK

IV. DEFORMABLE MIRROR OPERATION

Deformable mirrors correct aberrations in an optical imaging path by reshaping the optical wave-front. A Micro-Electro-Mechanical Systems (MEMS) deformable mirror is desirable because of its low cost, low power consumption, and compact size. The deformable mirror used in this experiment was manufactured by Boston Micromachines Corporation (BMC) and is made of a bendable surface that is stretched in a controllable manner by an array of electromechanical actuators driven by a control voltage. The actuator voltages are determined by response to feedback from an optical sensor in the imaging path, external to the DM [9].

A. BMC MIRROR SPECIFICATIONS

The BMC deformable mirror has an active actuator array size of 12 actuators by 12 actuators. The array forms an aperture of 3.3 mm by 3.3 mm. Although the array is 12 x 12, there are only 140 active actuators because the actuators in the 4 corners are stationary. The aperture can be flattened within a tolerance of 6.072 nm RMS. The maximum stroke of the DM is 1.8 μm which corresponds to the maximum operating voltage of 202 volts [10]. The DM is encased and stabilized in an interface box as shown in Figure 15.

Figure 15. Boston Micromachines deformable mirror in interface box (from [10]).

B. DM ELEMENT ACTUATION

Multiple means are available to control the individual actuation of each actuator on the deformable mirror.

1. Link UI

In order to confirm the proper functioning of the actuators, a user interface software package was provided by the manufacturer for the Multi-DM system. When individual elements are addressed in Link UI, they are ordered right to left, row by row in groups of 12 (see Figure 16).The software, called Link UI, can be used to apply voltage patterns, poke individual actuators, or apply user-defined voltage maps. Loading a user-defined voltage map is accomplished by loading a single column of voltages with the index corresponding to actuator position, and the voltage converted to hexadecimal values according to Equation (2)

$$V_{out} = \frac{300 * D}{65536} \tag{1}$$

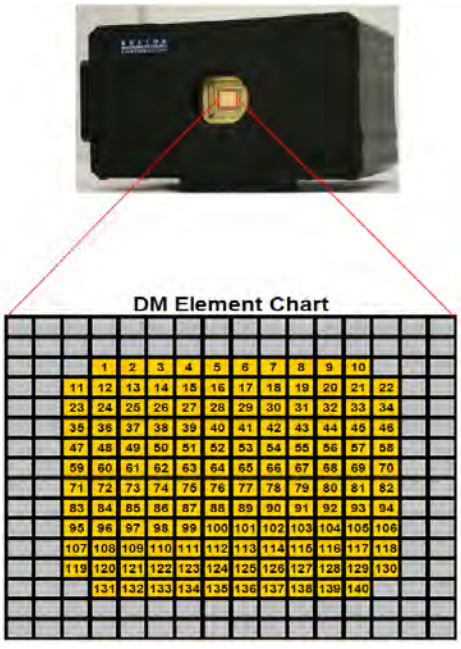

Figure 16. Actuator numbering (from [10]).

2. MATLAB Actuation

The BMC deformable mirror can be commanded utilizing MATLAB software. MATLAB version 7.4.0 (R2008b) and later releases contain *.mexw64 for 64-bit and *.mexw32 for 32-bit interface functions developed in C code that work in the Matlab environment. The Multi-DM "mex" functions require the Multi-DM driver software to be installed on the computer calling the functions utilizing input and return variables [10].

MATLAB commands the DM actuators with percentage control voltages, unlike the Link UI user interface which uses hexadecimal values of actual voltage. The input variable for actuator voltages is a 144 element vector of percent maximum driver voltages. All elements in the vector are required to be between 0 and 100, corresponding to 0 volts and max voltage (202 volts). There are 144 elements in the vector to provide a data set that is more easily manipulated in MATLAB. To accomplish this, the inactive corner actuators (1, 12, 133, and 144) are included in the vector and set to 0 as seen in Figure 17.

1	2	3	4	5	6	7	8	9	10	11	12
13	14	15	16	17	18	19	20	21	22	23	24
25	26	27	28	29	30	31	32	33	34	35	36
37	38	39	40	41	42	43	44	45	46	47	48
49	50	51	52	53	54	55	56	57	58	59	60
61	62	63	64	65	66	67	68	69	70	71	72
73	74	75	76	77	78	79	80	81	82	83	84
85	86	87	88	89	90	91	92	93	94	95	96
97	98	99	100	101	102	103	104	105	106	107	108
109	110	111	112	113	114	115	116	117	118	119	120
121	122	123	124	125	126	127	128	129	130	131	132
133	134	135	136	137	138	139	140	141	142	143	144

Figure 17. MATLAB actuator numbering with inactive corners (from [10]).

C. ACTUATOR DISPLACEMENT

In order to predict a deformable mirror shape that results from applied voltages, it is important to establish a relationship between applied voltage and resulting actuator

displacement. Predicting DM actuator response to known voltages can be challenging because the relationship between voltage applied and resulting displacement is non-linear. Additionally, the continuous face-sheet mirror exhibits mechanical coupling between actuators [9].

1. Actuator Design

Understanding the design and displacement method of MEMS deformable mirror actuators is critical for proper modeling and DM operation. Each DM actuator section, or sub-aperture, has a polysilicon actuator coated in aluminum at the top and a wired electrode at the bottom (see Figure 18). A polysilicon post is connected to the mirror surface actuator at the top and an actuator spring at the bottom. The DM actuator sub-apertures are separated by polysilicon/oxide walls. When a voltage is applied, the actuator is attracted to the electrode by an electrostatic force, thus pulling the mirror surface downward at the post connection. To return the mirror sub-aperture to its original position, the actuator spring provides a restoring force when the voltage is released [11].

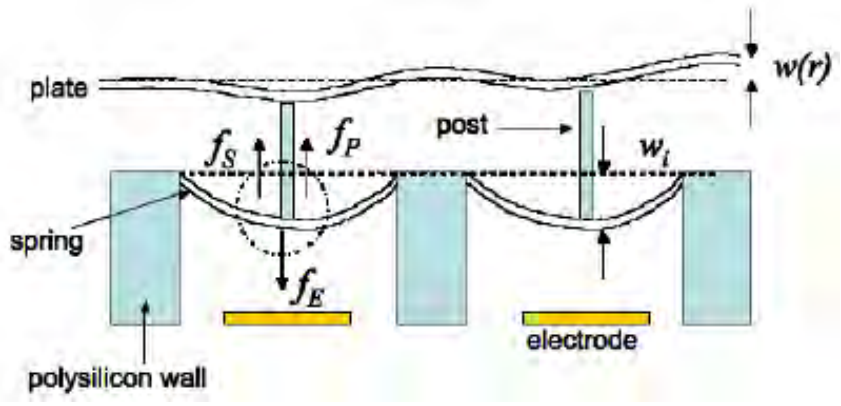

Figure 18. Two MEMS DM actuators in side view (from [11]).

2. Voltage to Displacement Experimental Data

After manufacturing, the performance of Boston Micromachines deformable mirrors are characterized prior to shipping, and the resultant voltage to displacement data curves are provided to the customer. The experimental data provided by BMC (see Figure

19) shows a quadratic relationship between the voltage applied and resulting actuator displacement. Single and 4x4 actuators are energized with the remaining actuators in an unpowered condition.

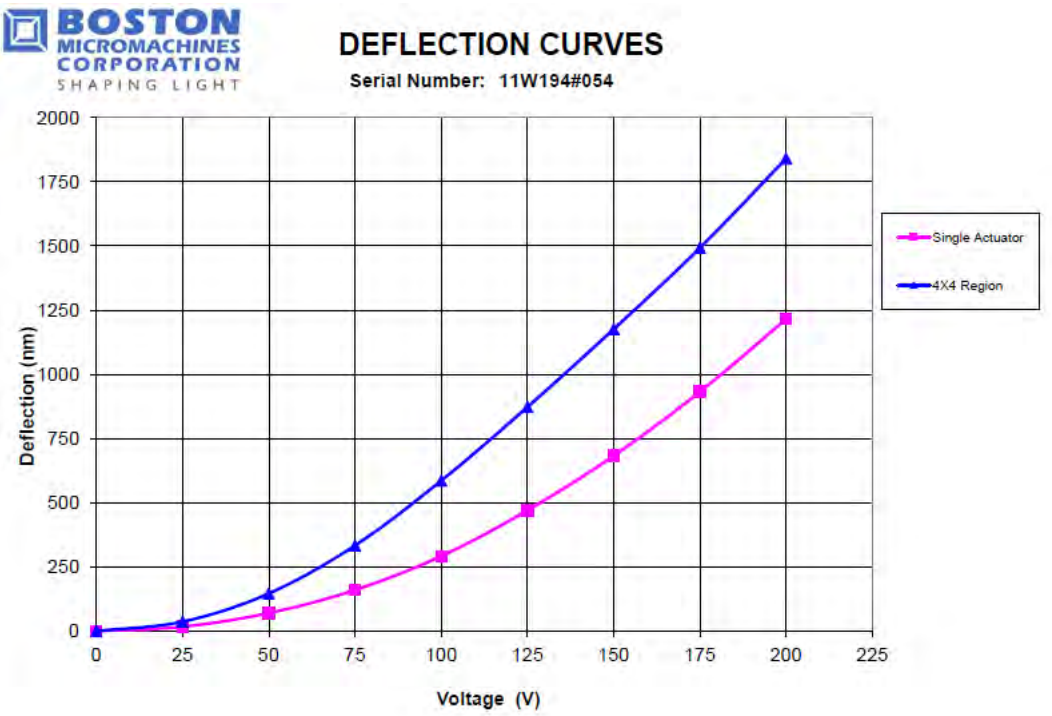

Figure 19. Manufacturer displacement vs. voltage curve (from [12]).

3. Curve Fitting Linear Relationship

In order to determine appropriate closed loop control for the deformable mirror actuators, a linear relationship must be established which relates desired actuator displacement to commanded actuator voltage. This relationship can be determined by curve-fitting the experimental data provided by the manufacturer. Utilizing the curve-fitting toolbox in MATLAB, a linear fit curve was found which can be used to approximate a linear relationship, as seen in Figure 20, which can be used in closed loop control.

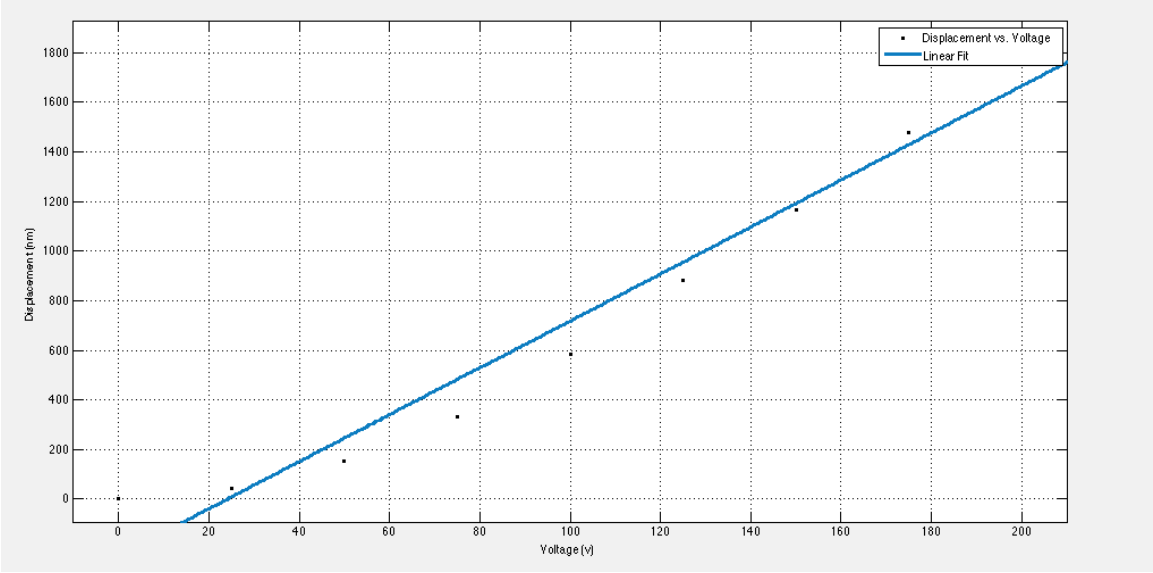

Figure 20. Linear fit for displacement vs. voltage.

The linear fit follows the 1st order polynomial relationship:

$$D = 9.478V - 228.6 \tag{2}$$

The actuator displacement (D) in nanometers and the voltage (V) in volts are now related in a way in which they can be commanded in a controllable manner.

V. CONTROL METHODS

The control method is the vital link between the surface figure sensor and the surface figure corrector, in this case, the deformable mirror. The first correction trial will utilize manual control to confirm the experimental set-up and gain intuition on general system properties. After this, an automated control method will be used in which a control algorithm will convert the surface figure aberration measurements made by the interferometer into a set of actuator commands that are applied to the deformable mirror to minimize the residual surface figure aberrations [13].

A. MANUAL CONTROL

1. Actuator Mapping

The position of the actuators that influence the surface figure of the segment can be determined experimentally. The individual actuator poke capability of the BMC LinkUI interface was used to command a near-maximum voltage pull on each actuator while viewing the segment position on the 4D interferometer 4Sight application in live video. The poke of the actuator causes an interference pattern in the live video that outlines the actuator location, as seen in Figure 21 and Figure 22.

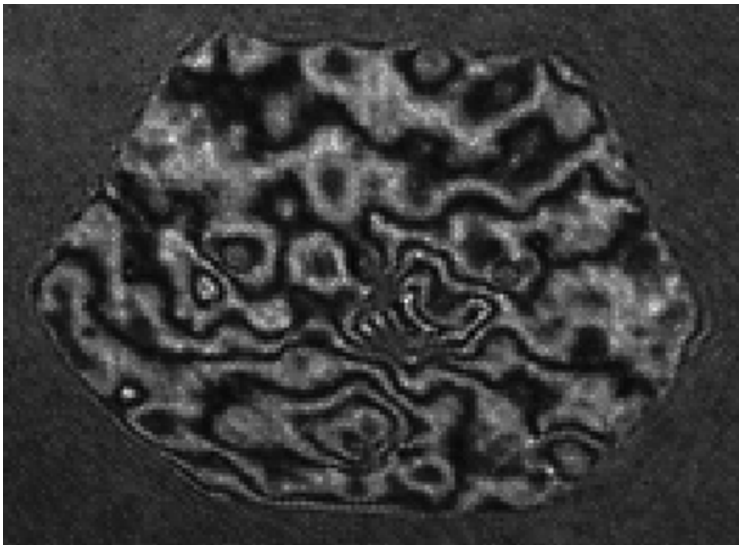

Figure 21. Interferometer image of segment without actuator commanded.

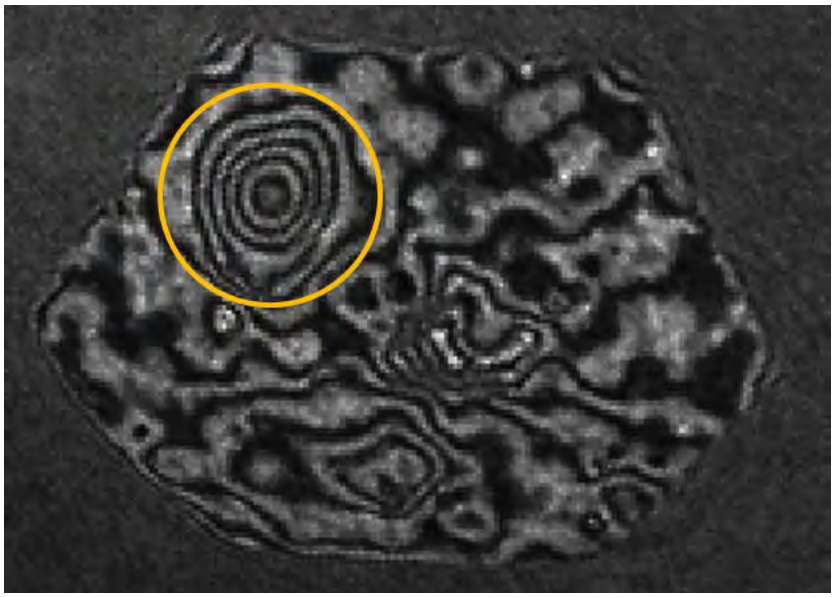

Figure 22. Interferometer image shows interference pattern when actuator is commanded.

The DM sub-assembly relay optics cause an image inversion that changes the positions of the DM actuators as they appear on the interferograms and live video. As a result, when viewing an aberration on the interferogram, the expected position of the corresponding actuator according to the BMC actuator mapping in Figure 17, is not correct. The new actuator locations with the relay inversion taken into account are mapped in Figure 23, so that aberration locations on the interferogram can be intuitively related to actuators that can be commanded.

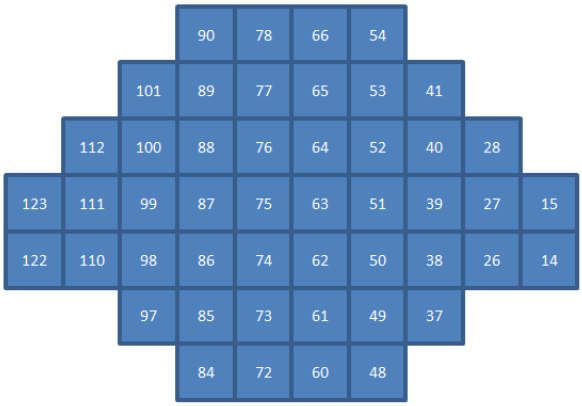

Figure 23. DM actuator inverted locations.

2. Manual Actuator Voltage Commands

The poke interface provided by BMC was not efficient in manual surface figure correction because it commands individual actuators with the rest of the deformable mirror remaining in an unpowered condition. The segment had both peak and valley aberrations to be corrected, so starting the deformable mirror from a flat condition with actuation distance forward and backwards was more advantageous. The 500nm flat file provided from the manufacturer was used as a starting point. After taking an interferogram of the baseline segment aberrations, the corresponding actuator was picked (see Figure 23) to make an adjustment. To command the actuator, the command value first had to read from the flat file in hexadecimal and then converted to decimal. After retrieving the decimal data word (D), the actual voltage could be found according to the relationship given in Equation 2 in Chapter IV.

$$V_{out} = \frac{300 * D}{65536} \tag{3}$$

After determining the actual voltage of the actuator that corresponds to the position of the aberration, a new desired voltage was determined based on whether the aberration was a peak or a valley. For peaks, the new desired voltage would be greater in order to pull the actuator backward from flat to reduce the peak. For valleys, the new desired voltage would be less in order for the actuator to have less voltage than the intermediate flat position so that it is in a forward from flat position to raise the valley.

After the new actuation voltage was determined, the same process as above would be followed in reverse to change the command value to the new desired value. The new desired decimal command data word (D) first needed to be determined.

$$D = \frac{65536 * V_{out}}{300} \tag{4}$$

After calculating a new decimal data word, the decimal was converted to hexadecimal to create the new final data word to command the actuator in the BMC deformable mirror software. The LinkUI software reads text files, so the new command for the individual actuator could replace the old command on the command file. Using load file

functionality, a set of commands for all 140 actuators would be actuated at once, with all actuators being in a flat condition except for those whose data words had been purposefully manipulated.

3. Manual Correction Iteration

After an aberration and the corresponding actuator were identified and commanded, the results from the new interferogram were saved. The process was repeated using the new interferogram as the new baseline. Each new command file was saved and indexed with the related interferogram. When the manual change made a performance improvement, the index and file became the new starting point. Using small incremental changes to handle one aberration at time was the most efficient method. Once a specific aberration was not progressing, another aberration on the surface figure became the new focus, using changes that were added to the previous successful index.

B. AUTOMATED CONTROL

1. Influence Matrix

In order to determine the relationship between the control voltage input and the related actuator movement, an influence function needs to be established. The influence function represents the deformable output as it relates to the action of a single actuator. If used in closed loop configuration, there is a tolerance for variations from linear behavior in the influence function [13]. Assuming linear relationship, the influence functions for the individual actuators are used to make an influence matrix for the entire mirror. The influence matrix is sometimes referred to as the "poke matrix."

2. Shack Hartmann Slope Influence Matrix

When developing influence matrix, the typical method used in adaptive optics is a slope influence matrix for use with a Shack Hartmann sensor. Although Shack Hartmann sensors are not used in this experiment, a brief explanation of the slope influence matrix used with Shack Hartmann sensors will be beneficial to eliminate confusion between traditional adaptive optics methods and the method used in this experiment.

In a basic slope influence matrix measurement procedure, the x and y displacements are measured on each Shack Hartmann sensor spot when a single actuator is commanded (see Figure 24). The Shack Hartmann wave-front sensor data from each actuator poke becomes a column in the actuator slope influence matrix. To build a complete actuator influence matrix, the procedure for each individual would be repeated to create a complete influence matrix. A control matrix can then be generated by calculating the pseudo-inverse of the influence matrix [13].

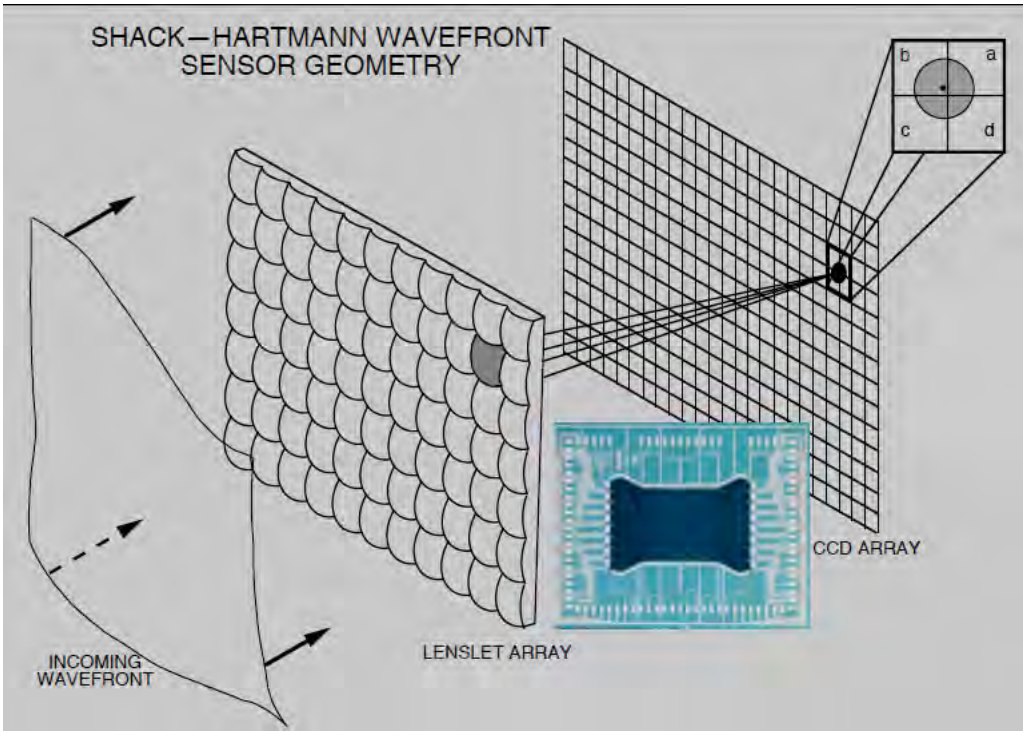

Figure 24. Shack Hartmann wave-front sensor measures slopes (after [14]).

3. Influence Function Using Interferometer

The Influence function that will be developed for this experiment is similar to the methodology used for Shack Hartmann sensor, but adapted for use with an interferometer. The influence will still be the relationship between the actuator input and sensor output in a linear equation of the form,

$$\mathbf{y} = \mathbf{\Phi u} \tag{5}$$

in which the input control is **u**, the influence matrix is $\mathbf{\Phi}$ and the output is **y**. The control input, **u,** can be any control variable that is calibrated to the DM actuators, and in this case will be control voltage, **V**. The output, **y,** can be any sensor output such as wave-front slope in the case of the Shack-Hartmann influence function from the previous chapter. For this experiment, the output will be the displacement, **D,** of the deformable mirror as measured by the phase difference readings of the 4D interferometer [15].

Three assumptions allow the influence matrix to be used for the system. The first assumption is that the actuator input and sensor output are both linear. The second is that when the actuator input is zero, the sensor output is zero. The third assumption is that DM dynamics are much faster than the rest of the system and sensor output values change to new values as soon as a new DM command is applied [15].

4. Determining the Influence Matrix

a. Calculating Poke Columns

The sensor output, **y**, provided by the 4D Interferometer is in the form of deformable mirror actuator displacement. The actuator input control, **u,** will be a vector with a maximum value of 1 and minimum value of -1.

$$\mathbf{u} = \begin{bmatrix} 1 \\ 0 \\ 0 \\ \vdots \\ 0 \end{bmatrix} \tag{6}$$

To experimentally determine the influence matrix, the vector control above will be applied to command a single actuator. The resulting output, **y,** from the 4D interferometer is a matrix of phase measurements that are equivalent to deformable mirror face displacements that result from the single actuator being commanded.

$$\mathbf{y} = \begin{bmatrix} \phi_{1,1} & \phi_{1,2} & \phi_{1,3} & \phi_{1,4} & \cdots & \phi_{1,n} \\ \phi_{2,1} & \phi_{2,2} & \phi_{2,3} & \phi_{2,4} & \cdots & \phi_{2,n} \\ \phi_{3,1} & \phi_{2,2} & \phi_{3,3} & \phi_{3,4} & \cdots & \phi_{3,n} \\ \phi_{4,1} & \phi_{3,2} & \phi_{4,3} & \phi_{4,4} & \cdots & \phi_{4,n} \\ \vdots & \vdots & \vdots & \vdots & \ddots & \vdots \\ \phi_{m,1} & \phi_{m,2} & \phi_{m,3} & \phi_{m,4} & \cdots & \phi_{m,n} \end{bmatrix} \tag{7}$$

Re-writing Equation 6 with the full expressions for **u** and **y** when only one actuator is commanded**,** the result is a single column vector that will comprise a single column of the influence matrix.

$$\begin{bmatrix} y_1 \\ y_2 \\ \vdots \\ \vdots \\ \vdots \\ y_m \end{bmatrix} = \begin{bmatrix} \phi_{1,1} & \phi_{1,2} & \phi_{1,3} & \phi_{1,4} & \cdots & \phi_{1,n} \\ \phi_{2,1} & \phi_{2,2} & \phi_{2,3} & \phi_{2,4} & \cdots & \phi_{2,n} \\ \phi_{3,1} & \phi_{2,2} & \phi_{3,3} & \phi_{3,4} & \cdots & \phi_{3,n} \\ \phi_{4,1} & \phi_{3,2} & \phi_{4,3} & \phi_{4,4} & \cdots & \phi_{4,n} \\ \vdots & \vdots & \vdots & \vdots & \ddots & \vdots \\ \phi_{m,1} & \phi_{m,2} & \phi_{m,3} & \phi_{m,4} & \cdots & \phi_{m,n} \end{bmatrix} \begin{bmatrix} 1 \\ 0 \\ 0 \\ 0 \\ \vdots \\ 0 \end{bmatrix} = \begin{bmatrix} \phi_{1,1} \\ \phi_{2,1} \\ \phi_{3,1} \\ \phi_{4,1} \\ \vdots \\ \phi_{n,1} \end{bmatrix} \tag{8}$$

This process is repeated to formulate the successive columns of the influence matrix by commanding successive actuators and collecting the sensor output. For instance, the next actuation would be a command column vector for the second actuator.

$$\mathbf{u} = \begin{bmatrix} 0 \\ 1 \\ 0 \\ \vdots \\ 0 \end{bmatrix} \tag{9}$$

The output that resulted from the command of the second actuator would be multiplied by the command vector in the same manner as was accomplished with the first actuator in order to create a column vector that forms the second column of the influence matrix.

$$\begin{bmatrix} y_1 \\ y_2 \\ \vdots \\ \vdots \\ \vdots \\ y_m \end{bmatrix} = \begin{bmatrix} \phi_{1,1} & \phi_{1,2} & \phi_{1,3} & \phi_{1,4} & \cdots & \phi_{1,n} \\ \phi_{2,1} & \phi_{2,2} & \phi_{2,3} & \phi_{2,4} & \cdots & \phi_{2,n} \\ \phi_{3,1} & \phi_{2,2} & \phi_{3,3} & \phi_{3,4} & \cdots & \phi_{3,n} \\ \phi_{4,1} & \phi_{3,2} & \phi_{4,3} & \phi_{4,4} & \cdots & \phi_{4,n} \\ \vdots & \vdots & \vdots & \vdots & \ddots & \vdots \\ \phi_{m,1} & \phi_{m,2} & \phi_{m,3} & \phi_{m,4} & \cdots & \phi_{m,n} \end{bmatrix} \begin{bmatrix} 0 \\ 1 \\ 0 \\ 0 \\ \vdots \\ 0 \end{bmatrix} = \begin{bmatrix} \phi_{1,2} \\ \phi_{2,2} \\ \phi_{3,2} \\ \phi_{4,2} \\ \vdots \\ \phi_{n,2} \end{bmatrix} \tag{10}$$

This process is repeated until all actuators have been commanded [15].

b. Constructing Influence Matrix in MATLAB

The influence matrix is composed column by column in MATLAB by taking interferograms for each actuator poke, and constructing the corresponding column in the influence matrix. If there is any tip, tilt, or piston in the data collected at the time of actuator poke, the poke column will contain false data creating a false relationship between that actuator poke and the false creation of tip, tilt, or piston in the mirror. Only data related to the poke of the actuator should be retained in order to make a correct association of the influence of each actuator on the sensor output. As such, a reference interferogram, as seen in Figure 25, with no actuators poked is first taken which can be subtracted from subsequent interferograms with actuators poked.

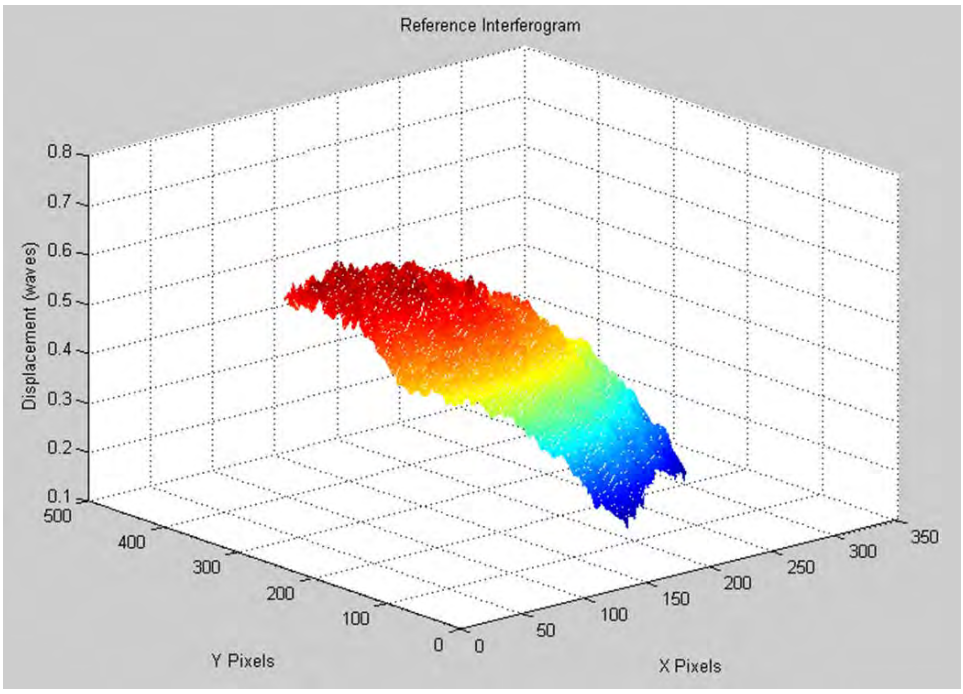

Figure 25. Reference interferogram with no actuators poked.

After collecting data from a reference interferogram with no actuators poked, all actuators in view of the segment are poked sequentially with interferometer sensor data collections for each poke. Before applying the tip, tilt, and piston correction, the data results will not have the appropriate accuracy to create poke columns that reflect the actuator's influence, as seen in Figure 26.

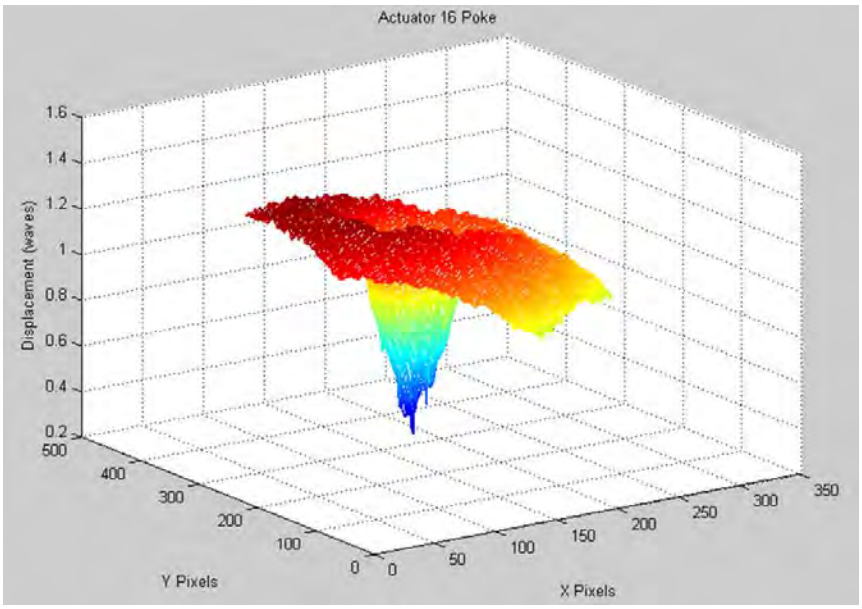

Figure 26. Interferogram data for Actuator 16 poke before tip, tilt, and piston correction.

Tip and tilt correction are applied by subtracting the reference interferogram data from the actuator poke data, as seen in Figure 27.

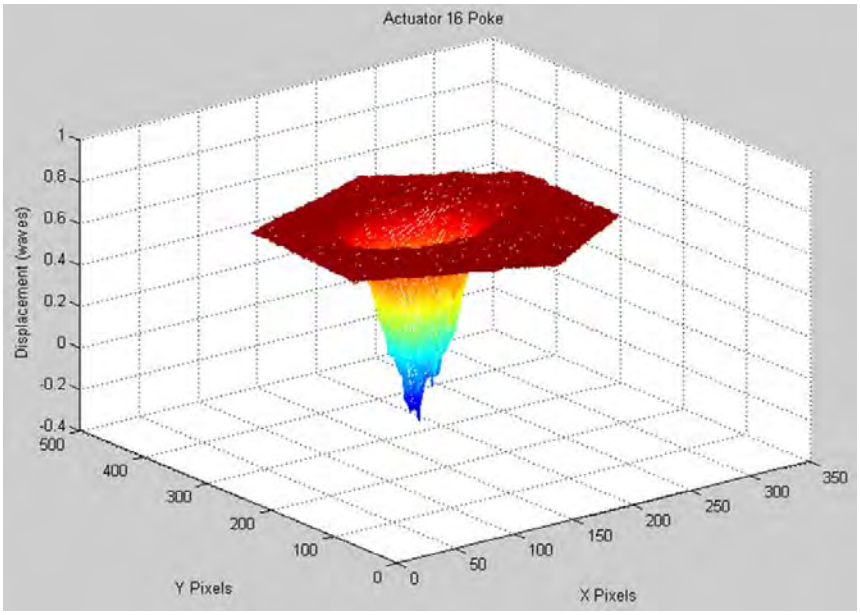

Figure 27. Interferogram data for Actuator 16 poke after tip and tilt correction.

After correcting tip and tilt, the arbitrary piston values that are assigned by the interferometer's 4Sight processing software can also be removed by subtracting a mean value, derived from the flat portion of the data. This piston adjustment is critical to ensure all poke data have the same reference point, and thus all columns create a coherent influence matrix. After correcting piston, tip, and tilt, the interferometer data from each actuator poke become the columns of the influence matrix. As such, the influence matrix will have the same number of columns as actuators that will be commanded. The mirror segment covers a section of the deformable mirror with forty-eight actuators, therefore the influence matrix has forty-eight columns. The interferometer is masked to only cover the mirror segment and provide the same number pixels of data for each collection. For the experimental configuration, the interferometer gathered 57,463 pixels for each data collection, thus the influence matrix has 57,463 rows. This being the case, the sensor data, from here on referred to as ϕ, will be a 57,463 element column vector.

$$\mathbf{\Phi}_{57463x48}\mathbf{u}_{48x1} = \phi_{57463x1} \tag{11}$$

In order to correlate results as new data sets are collected throughout the duration of the experiment, every sensor output which provides phase and displacement data, ϕ, must have dimensions 57463 x 1 for proper data manipulation and calculation.

C. CONTROL ALGORITHMS

1. Unconstrained Least Square Solution

After the sensor has determined the initial condition of the mirror segment, the mirror will be commanded utilizing the conjugate of the influence matrix. The required control is found by solving an unconstrained least square problem utilizing the pseudo-inverse of the Influence Matrix.

$$\mathbf{u} = \mathbf{\Phi}^{\dagger}\phi \tag{12}$$

The unconstrained least square solution is solved in MATLAB with a Moore-Penrose pseudo-inverse that seeks to minimize

$$\min_{\mathbf{u}} \frac{1}{2}\left\|\mathbf{\Phi}\cdot\mathbf{u}-\phi\right\|_2^2 \tag{13}$$

subject to no upper or lower bounds [16].

2. Constrained Optimization

In order to optimize the solution while remaining within the limits of the available control actuator displacement authority, a solution utilizing constrained optimization will solve least squares curve-fitting problems of the form

$$\min_{\mathbf{u}} \frac{1}{2}\left\|\mathbf{\Phi}\cdot\mathbf{u}-\phi\right\|_2^2 \text{ subject to } \text{lb} \le \mathbf{u} \le \text{ub}. \tag{14}$$

Constrained optimization was implemented using the lsqlin function in MATLAB [17]. The lower bounds and upper bounds were determined by calculating the remaining control space in the solution iteration.

3. Iterative Control with Linear Approximation

The control variable, **u**, requires a linear relationship to the sensor output. As stated in Chapter IV, the deformable mirror's quadratic behavior can be approximated as a first-order slope when small steps are used to remain in a linear range. As such, for purposes of a control algorithm, the control voltage (V) and the actuator displacement on the deformable mirror (D_{DM}) can be approximated such that

$$D_{DM} \propto cV \tag{15}$$

where c is a constant that scales the full range of voltages to maintain the control **u** in the range ($-1 \le \mathbf{u} \le 1$). Actuator displacements create corresponding phase shift displacements on the mirror segment, so a relationship is also established with displacement on the mirror segment.

$$D_{MS} \propto cV \tag{16}$$

The influence matrix also provided a relationship between control commands, **u**, and the phase shifts displacements on the mirror segment.

$$D_{MS} \propto \mathbf{u} \tag{17}$$

Therefore, taking all of the previous relationships into account, a relationship for control to commanded voltage is established.

$$\mathbf{u} \propto cV \tag{18}$$

Utilizing the 200nm flat file voltages supplied by the manufacturer, the value of c which provides optimal scaling was found to be c = .0286.

A control algorithm that utilizes voltage can be established for the deformable mirror to determine the voltage to be commanded while maintaining ($-1 \leq \mathbf{u} \leq 1$) and operating from a mid-point flat range on the deformable mirror.

$$\mathbf{v}(i) = \mathbf{u}(i) / c + \mathbf{v}_0 \tag{19}$$

where $\mathbf{v}_0$ is the voltage for the midway flat mirror starting point of the given actuator. Equation 20 can be applied iteratively in an unconstrained least square solution such that

$$\mathbf{u}(k+1) = \mathbf{u}(k) - K_i \mathbf{\Phi}^{\dagger} \phi(k) \tag{20}$$

The index of the control iteration is k and the iteration update gain is K_i [18]. For the constrained optimization solution, a similar relationship applies where β is the solution of the constrained optimization.

$$\mathbf{u}(k+1) = \mathbf{u}(k) - K_i \beta \tag{21}$$

THIS PAGE INTENTIONALLY LEFT BLANK

VI. RESULTS

A. MANUAL CORRECTION

1. Baseline Surface Figure

The mirror segment used in the manual correction experiment showed a prominent peak, a distinct valley, and a less prominent valley before correction. The 4Sight software that renders the 4D interferometer data displays high spots, or peaks, in red, and low spots, known as valleys, in blue. Performance characteristics of the mirror surface figure are calculated in the 4D interferometer software and the level of surface aberration is calculated in root mean square (RMS). A peak to valley (PVq) calculation is also provided with Q=99% for the highest and lowest spot on the surface. The performance characteristics of the baseline surface figure are shown in Figure 27 and Table 1.

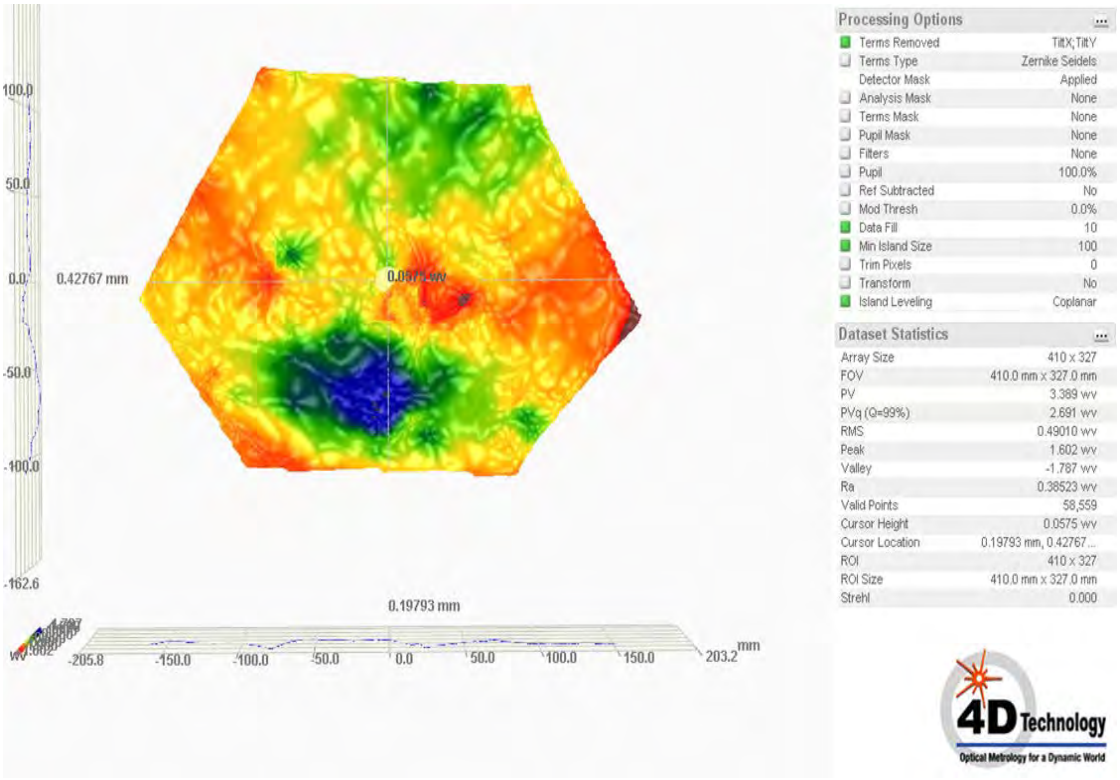

Figure 28. Mirror segment with aberrations before manual correction.

Interferometer Surface Figure Data		
RMS	0.49	waves
Peak to Valley (PVq)	2.69	waves

Table 1. Performance before manual correction.

2. Prominent aberration targeting

When correcting manually, it would at first seem prudent to completely remove the large peak aberration from the mirror in order to improve overall performance. However, removing the large peak required large actuator movement in a localized area with the rest of mirror remaining unpowered to achieve the required stroke displacement. Therefore, counter to intuition, the actuator movement required to remove the large peak resulted in an overall lower performance of the mirror surface figure, as seen in Figure 28 and Table 2.

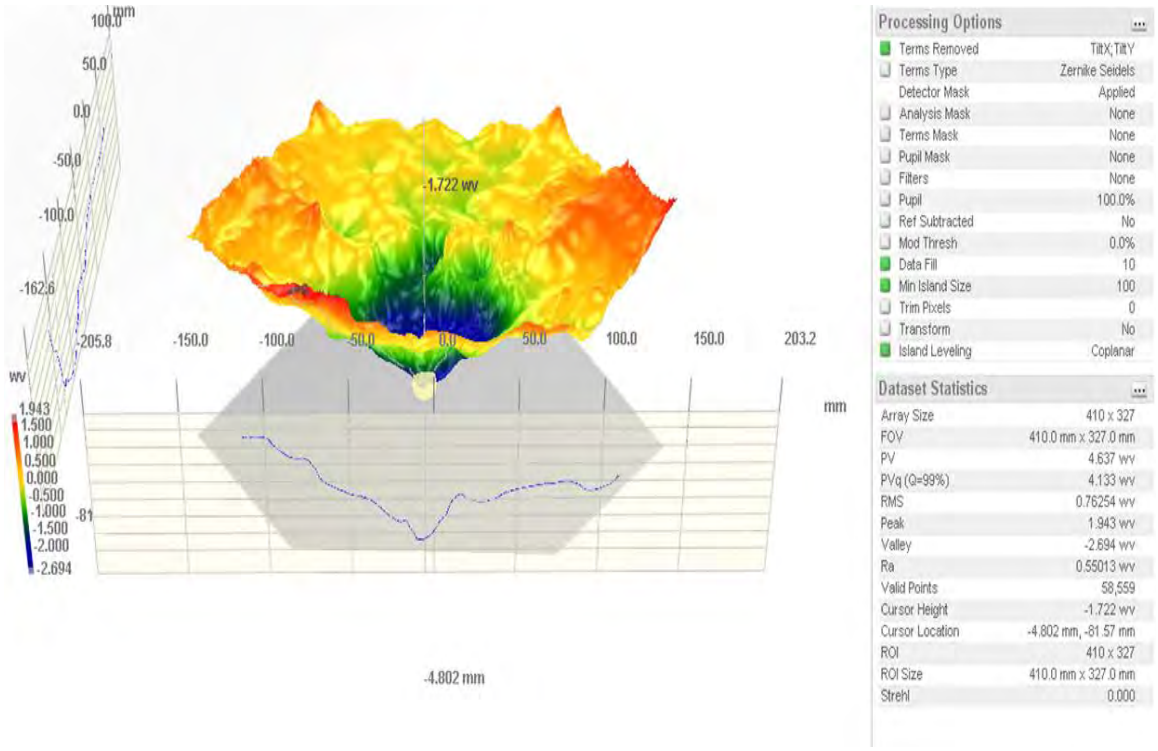

Figure 29. 3-D side view of middle peak removal resulting in poor overall performance.

Interferometer Surface Figure Data		
RMS	0.76	waves
Peak to Valley (PVq)	4.13	waves

Table 2. Surface Figure degradation.

3. Localized Small-Step Iterations

The most efficient method of manual correction proved to be local targeting of aberrations with small iterations of 20 volt actuator commands. Even if a large aberration was still visible, a new area would be targeted holding the current target best value constant after performance characteristics began to degrade in the current target area. This methodology led to the best results as seen in Figure 29 and Table 3.

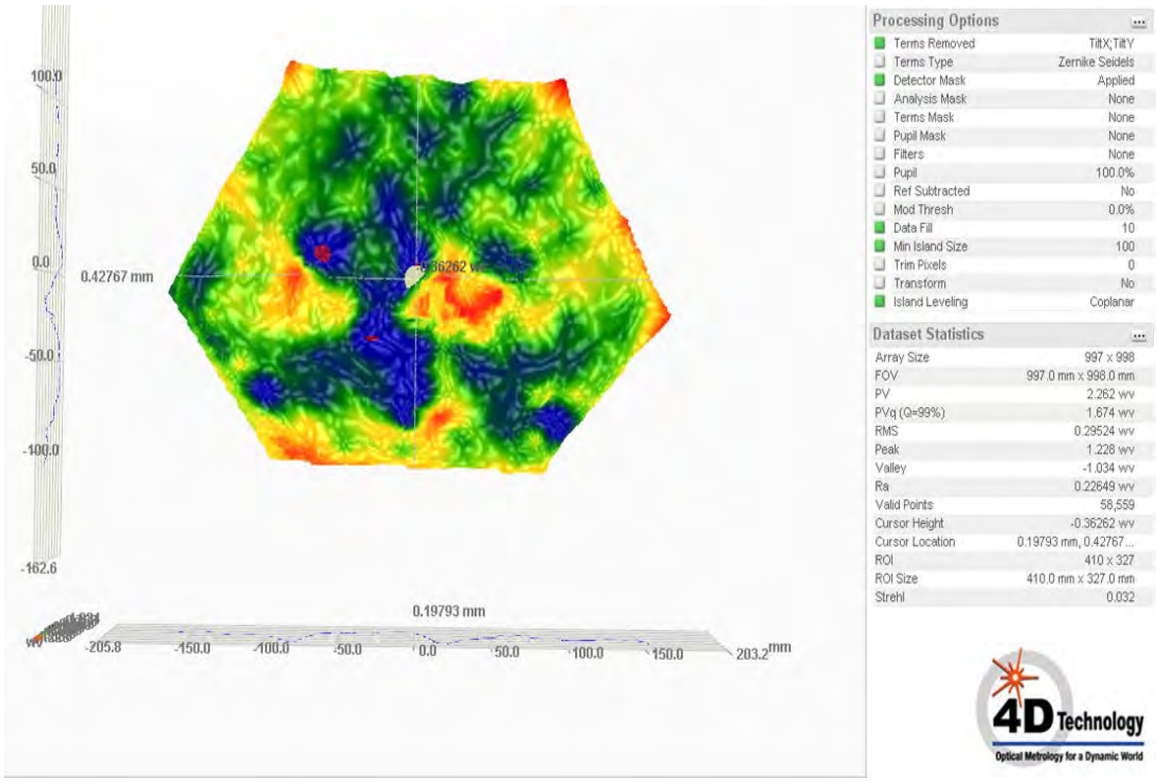

Figure 30. Best manual results were achieved using small steps.

Interferometer Surface Figure Data		
RMS	0.29	waves
Peak to Valley (PVq)	1.67	waves
% Change RMS	40%	improvement
% Change PVq	38%	improvement

Table 3. Manual correction performance improvement.

B. AUTOMATED CONTROL CORRECTION

1. Iterative Feedback Method

a. Baseline Prior to Correction

After the manual method, every subsequent automated correction sequence begins with a new interferometer baseline picture to ensure accuracy in data collection. In-room atmospheric disturbance, thermal conditions, and physical drift in the laboratory can affect the starting point of observation due to the minute nature of nanometer-level aberrations. As such, each experimental sequence starts with a new baseline for comparison. The performance characteristics of the mirror segment prior baseline surface figure used in the pseudo-inverse method are shown in Figure 30 and Table 4. Prior to correction, the segment showed very prominent peaks and valleys.

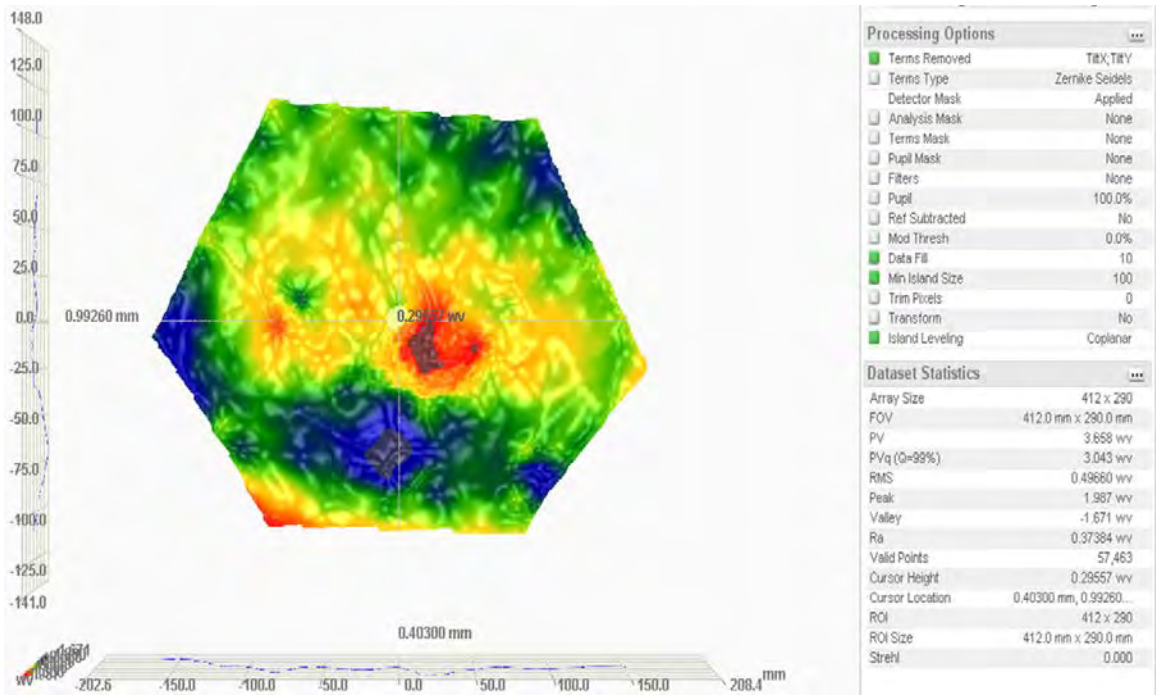

Figure 31. Baseline mirror segment with prominent peak and valley prior to correction.

Interferometer Surface Figure Data		
RMS	0.49	waves
Peak to Valley (PVq)	3.04	waves

Table 4. Baseline surface figure quality prior to iterative feedback correction.

b. Surface after Iterative Feedback correction

The prominent peaks and valleys were removed by direct Iterative Feedback correction after nine iterations. A gain value of Ki=0.1 provided a gradual approach to minimizing the peak and valleys. The improved surface figure data are given in Figure 31 and Table 5.

Interferometer Surface Figure Data		
RMS	0.23	waves
Peak to Valley (PVq)	1.53	waves
% Change RMS	54%	improvement
% Change PVq	50%	improvement

Table 5. Iterative feedback method provides better results than manual correction.

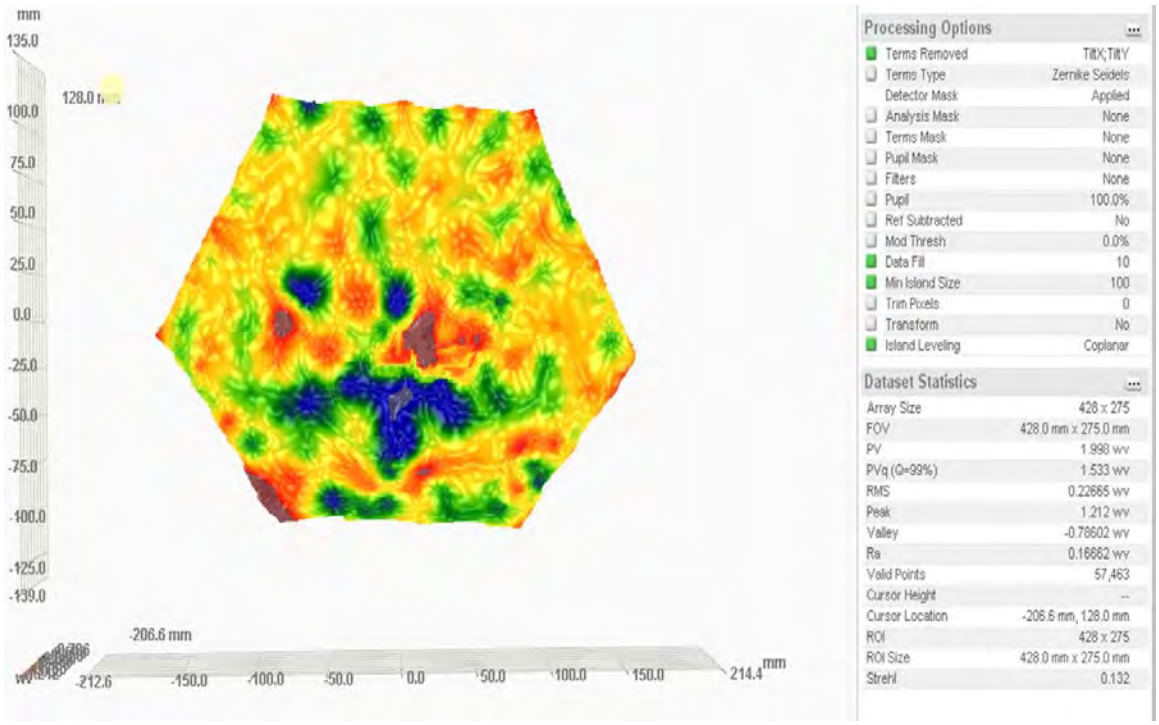

Figure 32. Peaks and valleys were minimized by iterative feedback control.

2. Iterative Feedback with Constrained Optimization

a. Baseline Surface Figure

Prior to applying an Iterative Feedback with Constrained Optimization (IFCO), the interferometer showed the mirror surface as having a poor surface figure. Table 6 and Figure 32 provide data for the mirror starting point before correction.

Interferometer Surface Figure Data		
RMS	0.54	waves
Peak to Valley (PVq)	3.06	waves

Table 6. Mirror surface prior to IFCO correction.

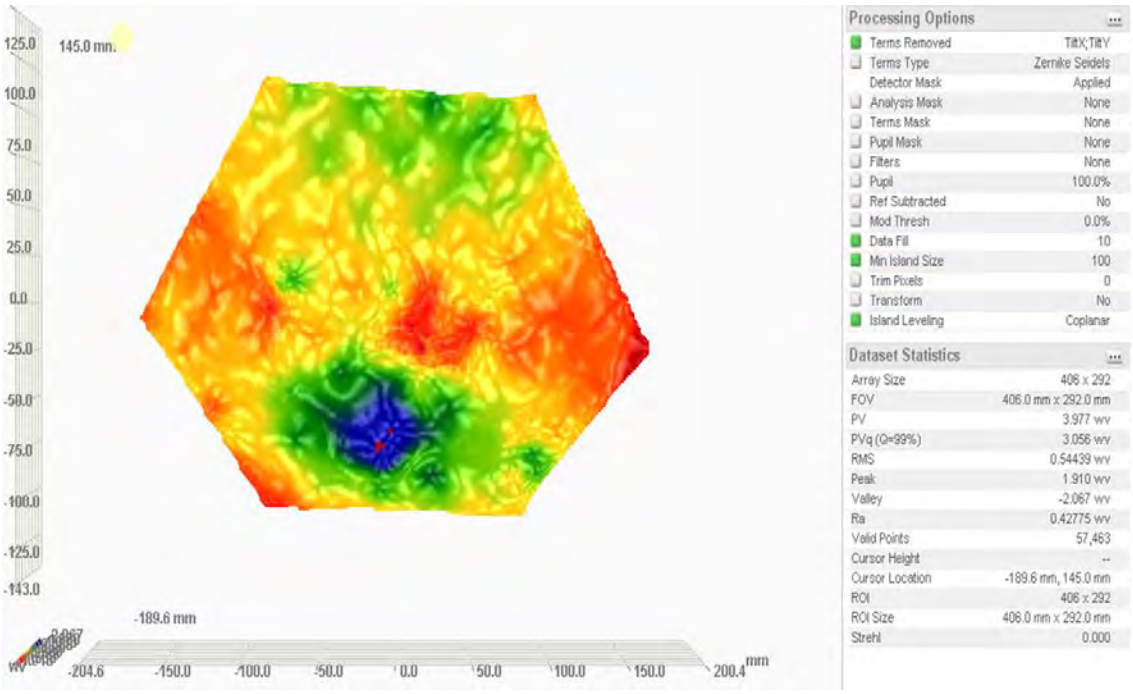

Figure 33. Mirror surface prior to IFCO correction with prominent peaks and valleys.

b. Surface after Iterative Feedback with Constrained Optimization Correction

Utilizing iterative feedback, the surface figure was improved over 12 iterations until it reached a point close to pervious best results of 1.6 waves PVq and .26 waves RMS. After this, the constrained optimization approach was applied with the constrained bounds being the remaining control authority in the deformable mirror actuators. The constrained optimization provided slightly more mirror surface figure correction beyond that of just iterative feedback as it solved for the optimal solution of removing remaining aberrations with available actuator positions and displacement. Of the three methods, iterative feedback with constrained optimization had the best relative surface figure improvement of 55% waves RMS, as seen in Table 7 and Figure 33.

Interferometer Surface Figure Data		
RMS	0.25	waves
Peak to Valley (PVq)	1.47	waves
% Change RMS	55%	improvement
% Change PVq	52%	improvement

Table 7. IFCO control method provides best results.

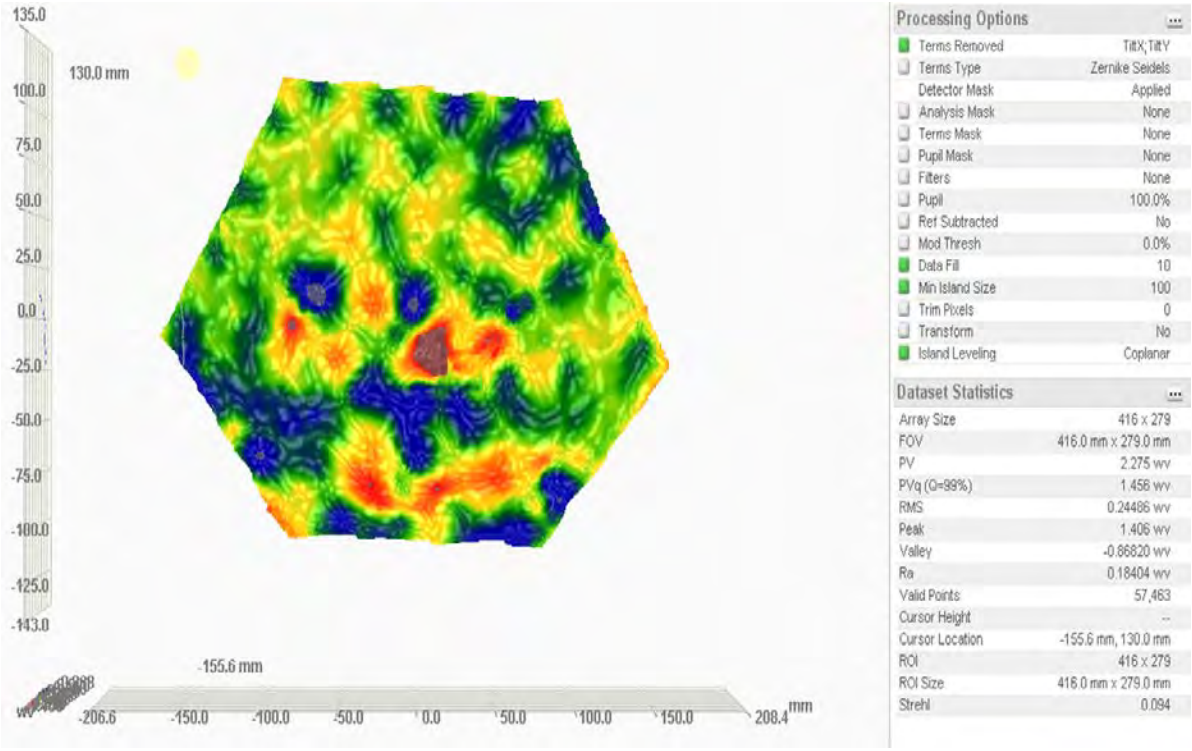

Figure 34. IFCO control method minimized peaks and valleys for best results.

VII. CONCLUSIONS AND FUTURE WORK

A. CONCLUSIONS

1. Successful Mirror Surface Figure Correction

This research has shown that a deformable mirror can be used to correct the mirror surface figure of a segmented mirror imaging system. Using the medium performance BMC deformable mirror procured for the experiment, 55% RMS improvement for the mirror surface was achieved. A higher spatial resolution deformable mirror should be capable of higher resolution improvement, thus providing better overall RMS correction. This research provides a proof-of-concept of the ability to remotely correct a mirror surface figure on orbit that will result in a higher level of confidence to launch a segmented mirror imaging satellite in the future.

2. Control Methods

An Iterative Feedback control method combined with late iteration Constrained Optimization is the most efficient means of controlling the deformable mirror. In all cases, small gains ($Ki \leq 0.3$) allowed for gradual approach to a solution with minimum overshoot. When larger gains were utilized, the solution was too aggressive, resulting in larger aberrations on the mirror surface.

B. FUTURE WORK

1. Higher Resolution Deformable Mirror

The current DM sub-assembly could be upgraded by procuring a higher spatial resolution deformable mirror. With higher spatial resolution, aberrations on the mirror surface that are tightly spaced could be more efficiently handled by the control algorithm and hardware. With a higher spatial resolution deformable mirror, high peaks and low valleys that are spatially close could be individually corrected if the deformable mirror actuator pixels are smaller than the areas to be corrected.

2. Apply DM Technique to Carbon Composite Mirror

Carbon fiber reinforced polymer (CFRP) mirrors offer ultra-light and inexpensive solutions for imagery applications, but the mirror surface quality is currently not high enough for optical orbital imagery systems [19]. The same technique used in this experiment to improve the surface figure of a segmented mirror could be applied to a CFRP mirror to improve the surface figure quality. A CFRP mirror integrated with a deformable mirror could be tested as an inexpensive, high performance satellite imagery primary optic solution.

APPENDIX MATLAB CODE

```
%Code to Create Phi Matrix

ref_file_name = 'C:\Documents and Settings\Administrator\Desktop\Jae Stuff\4Sight Data\channel_00c.h5';
dataset = '/measurement0/genraw/data';
data_ref = h5read(ref_file_name, dataset);
data_ref = double(data_ref(281:693,631:933));
for i = 1:413
   for j = 1:303
      if data_ref(i,j) > 300
         data_ref(i,j) = NaN;
      else
         data_ref(i,j) = data_ref(i,j);
      end
   end
end


close all
clear phi_correct
file_name = 'C:\Documents and Settings\Administrator\Desktop\Jae Stuff\4Sight Data\channel_48c.h5';
dataset = '/measurement0/genraw/data';
data = h5read(file_name, dataset);
data = double(data(281:693,631:933))-data_ref;
for i = 1:413
   for j = 1:303
      if data(i,j) > 300
         data(i,j) = NaN;
      else
         data(i,j) = data(i,j);
      end
   end
end

phi = [];
for i = 1:413
   for j = 1:303
      if ~isnan(data(i,j))
         phi = [phi;data(i,j)];
      end
   end
```

```
end

imagesc(data)
figure,mesh(data)
figure,plot(phi)


tmp = mean(phi(10000:53000))
phi_correct = phi-tmp;
figure,plot(phi_correct)
save phi_data_48 data_ref data phi phi_correct



%Code to Create Influence Matrix

function influence_matrix = create_influence_matrix(varargin)

%influence_matrix = create_influence_matrix(varargin)
%This function creates influence matrix from the saved data

n = 48; % number of DM channels that affect the segment
for i = 1:n;
   file_name = strcat('phi_data_',sprintf('%d',i));
   load(file_name);
   influence_matrix(:,i) = phi_correct; % poke matrix
   mesh(data);
   drawnow;
end


%Code to Command DM

function [success] = command_DM(u)

% [varargout] = command_DM(u)
% This function commands the deformable mirror with command u

% import hex flat biased file and read hex numeric using %x file format conversion (Scan
an integer as an unsigned hexadecimal number)
% Use 140 as the size and add 4 zeros at the corners for actual command
%fid = fopen('flat_biased_hex_voltage.txt'); %500nm flat file
fid = fopen('hex_flat200nm.txt'); %200nm flat file
flat_volt = fscanf(fid,'%x', 140);
```

```
per_flat_volt =  flat_volt/65536*100; % convert the flat voltage in 16 bit number to percentage
fclose(fid);

% convert u to percentage voltage (u = c(v-v0)^2 or v = sqrt(u/c)+v0
% u_full = u; % relationship between u (36x1) to u_full (140x1) (DETERMINE!!!!!!!!!!!)

u_full = zeros(140,1);
u_full(26:27) = u(1:2);
u_full(37:40) = u(3:6);
u_full(48:53) = u(7:12);
u_full(60:65) = u(13:18);
u_full(72:77) = u(19:24);
u_full(84:89) = u(25:30);
u_full(97:100) = u(31:34);
u_full(110:111) = u(35:36);
u_full(14:15) = u(37:38);
u_full(28) = u(39);
u_full(41) = u(40);
u_full(54) = u(41);
u_full(66) = u(42);
u_full(78) = u(43);
u_full(90) = u(44);
u_full(101) = u(45);
u_full(112) = u(46);
u_full(122:123) = u(47:48);

c = 1/35; %scaling relationship between u and percentage voltage u = c(v-v0)^2
v = zeros(140,1); %initialize the voltage command

% assuming quadratic relationship
% for i = 1:140
%     if u_full(i) >= 0,
%         v(i) = (sqrt(u_full(i))/c)+per_flat_volt(i);
%     else
%         v(i) = -(sqrt(-u_full(i))/c)+per_flat_volt(i);
%     end
% end

% assuming linear relationship
for i = 1:140
v(i) = u_full(i)/c+per_flat_volt(i);
end
```

```
% Set default Mult-Dm file to generation 2, MultiDM-01
% Mapping_ID =2 for "MultiDM-01" configuration.
mapping_ID = 2;
[error_code, driver_info] = OPEN_multiDM(mapping_ID);
v_actual = [0; v(1:10); 0; v(11:130); 0; v(131:140); 0];
UPDATE_multiDM(driver_info, v_actual);
success = ~error_code;

% Disable and close Multi=DM driver USB connection
%error_code = CLOSE_multiDM(driver_info);


%Code to create upper and lower CO bounds

A_bd=eye(48);
b_bd=ones(48,1);
ub = b-u;
lb = -b - u;



%Code to run correction iterations

%load phi_matrix

%Activate below 2 lines for starting new run
u0 = zeros(48,1);
u_prev = u0;

%command_DM(u_prev);

ref_file_name = 'C:\Documents and Settings\Administrator\Desktop\Jae Stuff\4Sight
Data\channel_00c.h5';
dataset = '/measurement0/genraw/data';
data_ref = h5read(ref_file_name, dataset);
data_ref = double(data_ref(281:693,631:933));
for i = 1:413
   for j = 1:303
      if data_ref(i,j) > 300
         data_ref(i,j) = NaN;
      else
         data_ref(i,j) = data_ref(i,j);
      end
   end
end
```

```
file_name = 'test_data.h5';
dataset = '/measurement0/genraw/data';
data = h5read(file_name, dataset);
data = double(data(281:693,631:933));%-data_ref;
for i = 1:413
   for j = 1:303
      if data(i,j) > 300
         data(i,j) = NaN;
      else
         data(i,j) = data(i,j);
      end
   end
end

data_tt = remove_tiptilt(data);

phi = [];
for i = 1:413
   for j = 1:303
      if ~isnan(data_tt(i,j))
         phi = [phi;data_tt(i,j)];
      end
   end
end
phi = phi-mean(phi);



%delta_u = pinv_phi*phi;

%A_bd=eye(48);
%b_bd=ones(48,1);

%lb = -ones(48,1);
%ub = ones(48,1);

ub = b_bd - u;
lb = -b_bd - u;

delta_u = lsqlin(influence_function,phi,A_bd,b_bd,[],[],lb,ub);

%phi contains last interferogram output to be corrected

u = u_prev-0.1*delta_u;
```

```
for i = 1:length(u)
   if u(i) >= 1
      u(i) = 1;
   elseif u(i) <= -1
      u(i) = -1;
   else
      u(i) = u(i)
   end
end

command_DM(u)
u_prev = u;


%Code for collecting poke data automatically

%Set basic parameters. This is for Boston Micro Multi-CDM 12x12 DM
%actuator number for actuators vector (144) in MATLAB
num_actuators = 144;

%Set default Mult-Dm file to generation 2, MultiDM-01
mapping_ID = 2;
[error_code, driver_info] = OPEN_multiDM(mapping_ID);

% Import hex flat file
fid = fopen('C:\Program Files\Boston Micromachines\Usb\CIUsbLib\hex_11W194#54_Final_CLOSED_LOOP_VOLTAGES.txt');

% Reads hex numeric using %x file format conversion. Use 140 as the
% size because the Multi-Dm does not include the 4 corners in the vector
% for the driver software. The zeros will be added later for the MATLAB
% version which includes the corners
act_flat_dec = fscanf(fid,'%x', 140);
fclose(fid);

%Convert the decimal flat voltage file to percentage for MATLAB use
%See pg 7 User manual

act_flat_base =  act_flat_dec/65536 * 100;

%Insert zeros for corners to make 144 element vector, as needed
%for MATLAB control
```

```
act_flat_base = [0; act_flat_base(1:10); 0; act_flat_base(11:130); 0;
act_flat_base(131:140); 0];

%Send Flatten DM command using percentage voltages and pause
UPDATE_multiDM(driver_info, act_flat_base);

pause(5);

%Set to flat minus 50% voltage, then back to zero for all actuators

%vector of voltage zeros to start with
act_volt = zeros(num_actuators,1);

numberOfFiles=42;

%Determine the control voltage -1 < u < 1
%u = -1;

%Determine scaling factor for voltage, in percentage voltage
%Actual voltage Range is 166.2 to 193.4 for segment usable area of DM face
%((166.2+193.4)/2) /202 = .89

%c = 100; %adjust this later. Maybe use 200nm flat file values also

%The control voltage to be added to the individual actuator

%v_control = u*c
v_control = 10;

%Don't actuate 1, 12, 133, 144 actuators
for i = [17:18,28:31,39:44,51:56,63:68,75:80,87:92,100:103,113:114]
   %if i ~= 12 || i ~= 133 not necessary b/c not poking all actuators

      %Add control voltage to indexed actuator
      act_volt(i,1) = act_volt(i,1) + v_control;
      actset = act_volt + act_flat_base;
      UPDATE_multiDM(driver_info, actset);
         tic
          fid = fopen(['C:\4DScriptRunner\script_' num2str(i)  '.py'], 'wt');


          fprintf(fid, 'from Scripting.App import *\n');
          fprintf(fid, 'from Scripting.Data import *\n');
          fprintf(fid, 'from Scripting.Measurements import *\n');
          fprintf(fid, 'from Scripting.Modify import *\n');
```

```
        fprintf(fid, 'n = 1\n');
        fprintf(fid, 'm = Measure()\n');

%           fprintf(fid, 'm2 = m.GetRawDataset()\n');
%           fprintf(fid, 'RemovePiston(m2)\n');

        fprintf(fid, 'm2 = m.GetAnalyzedDataset()\n');
        fprintf(fid,                'SaveMeasurement(m2,"C:/Documents                and
Settings/Administrator/My
Documents/Deformable_Mirror/Actuators_42_10percent_Oct13/BMC_Actuator_%d.h5"
)\n', i);
        fprintf(fid, 'del m\n');
        fclose(fid);
        disp(['Iteration ' num2str(i) '/' num2str(numberOfFiles) ' complete']);


toc

%       act_volt(i,1) = act_flat_base(i,1);
    act_volt = zeros(num_actuators,1);
    UPDATE_multiDM(driver_info, actset);

    while(exist(['C:\4DScriptRunner\script_' num2str(i)  '.py'],'file'))
       pause(0.5);
    end
    pause(2)

  end



% Disable and close Multi=DM driver USB connection
error_code = CLOSE_multiDM(driver_info);

% Obtaining and plotting the data. Not currently used so commented.
% for j = 61:69
%    if j ~= 12 || j ~= 133
%       % This section will obtaind and plot the data from the *.h5 file
%       %
%       filename=(['BMC_Actuator_' num2str(j) '.h5'])
%       D4_data=hdf5read(filename, '/measurement0/genraw/data');
%       for z1=1:997
%          for z2=1:998
%             if(D4_data(z1,z2) > 100000)
%                D4_data(z1, z2)=NaN;
```

```
%               end;
%            end;
%        end;
%
%        disp(['D3 Dataset Statistics Peak=' num2str(max(max(D4_data))*0.6328)])
%        file_mat=(['BMC_Data_poke'  num2str(j)  '.mat']);
%        save(file_mat, 'D4_data')
%        figure;
%        mesh(double(D4_data));
%        imagesc((D4_data));
%     end
% end
```

THIS PAGE INTENTIONALLY LEFT BLANK

LIST OF REFERENCES

[1] A. Yingling, "Integrated optics, structures, and controls of segmented mirror telescopes," Ph.D. dissertation, MAE, NPS, Monterey, CA, 2012.

[2] J. M. Howard, "Optical Modeling Activities for the James Webb Space Telescope (JWST) Project: 1. The Linear Optical Model," in *Optical Modeling and Performance Predictions Conf.,* San Diego, CA, 2004, Proc. SPIE, vol. 5178, pp. 82–88.

[3] T. W. Axtell, "Segmented mirror telescope model and simulation," M.S. Thesis, MAE, NPS, Monterey, CA, 2011.

[4] K. Doyle, V. Genberg, and G. Michels, *Integrated Optomechanical Analysis*, 2nd ed. Bellingham, WA: SPIE Press, 2012.

[5] J. Bagnasco, private communication, Jan. 2013.

[6] J. Bagnasco, "Status Report for Support Research for the Adaptive Optics Center of Excellence," Naval Postgraduate School, 2013, unpublished.

[7] Office of the Chief NASA Technologist. (2011, May). Interferometers Sharpen Measurements for Better Telescopes." [Online]. Available: http://spinoff.nasa.gov/Spinoff2012/ip_7.html.

[8] J. Bagnasco, "SMT Experiment," Naval Postgraduate School, 2013, unpublished.

[9] Y. Zhou and T. Bifano, "Adaptive optics using a MEMS deformable mirror," in *Proc. 5th International Workshop on Adaptive Optics for Industry and Medicine*, Beijing, China, 2005, pp.171-177.

[10] *Multi-DM Deformable Mirror System User Manual*, V.3.4.3 Rev G, Boston Micromachines Corporation, Boston, MA, 2012.

[11] K. M. Morzinski, K. B. W. Harpsøe, D. T. Gavel, and S. M. Ammons, "The open-loop control of MEMS: modeling and experimental results," Proc. *SPIE*, vol. 6467, p. 64670, Feb. 2007.

[12] *Multi-CDM System Data Sheet*, Boston Micromachines Corporation, Boston, MA, Feb. 2013.

[13] J. Porter, H. Queener, K. Thorn, and A. Awwal, *Adaptive Optics for Vision Science*. Hoboken, NJ: John Wiley and Sons, 2006, ch. 7, pp. 155-187.

[14] R. Q. Fugate, "Adaptive Optics," presented at the Adaptive Optics Conf., Monterey, CA, 2012.

[15] J. J. Kim, “Influence Function and Influence Matrix,” Naval Postgraduate School, 2013, unpublished.

[16] *MATLAB Primer,* Mathworks, Inc., Natick, MA, 2013.

[17] *MATLAB User’s Guide,* Mathworks, Inc., Natick, MA, 2011.

[18] J. J. Kim, private communication, Oct. 2013.

[19] P. Sergio and J. Steeves, “Ultra-thin highly deformable composite mirrors,” presented at the Structures, Structural Dynamics, and Materials Conference, Boston, MA, 2013.

INITIAL DISTRIBUTION LIST

1. Defense Technical Information Center
   Ft. Belvoir, Virginia

2. Dudley Knox Library
   Naval Postgraduate School
   Monterey, California